
Electronic Thesis and Dissertation Repository

12-2-2013 12:00 AM

The Effective Dose of Different Scanning Protocols Using the Sirona Galileos® Comfort CBCT Scanner

David R. Chambers, *The University of Western Ontario*

Supervisor: Dr. Richard Bohay, *The University of Western Ontario*

Joint Supervisor: Dr. Jerry Battista, *The University of Western Ontario*

A thesis submitted in partial fulfillment of the requirements for the Master of Clinical Science degree in Orthodontics

© David R. Chambers 2013

Follow this and additional works at: <https://ir.lib.uwo.ca/etd>



Part of the [Other Dentistry Commons](#)

Recommended Citation

Chambers, David R., "The Effective Dose of Different Scanning Protocols Using the Sirona Galileos® Comfort CBCT Scanner" (2013). *Electronic Thesis and Dissertation Repository*. 1877.
<https://ir.lib.uwo.ca/etd/1877>

This Dissertation/Thesis is brought to you for free and open access by Scholarship@Western. It has been accepted for inclusion in Electronic Thesis and Dissertation Repository by an authorized administrator of Scholarship@Western. For more information, please contact wlsadmin@uwo.ca.

**THE EFFECTIVE DOSE OF DIFFERENT SCANNING PROTOCOLS USING THE
SIRONA GALILEOS® COMFORT CBCT SCANNER**
(Thesis format: Monograph)

by

David Chambers

Graduate Program in Orthodontics

A thesis submitted in partial fulfillment
of the requirements for the degree of
Master of Clinical Dentistry

The School of Graduate and Postdoctoral Studies
The University of Western Ontario
London, Ontario, Canada

© David Chambers 2014

Abstract

Introduction: Cone Beam CT imaging is prevalent in dentistry yet much is unknown with regard to how radiation dose to the patient varies between different CBCT scanners and imaging protocols. Scanner and protocol specific effective dose calculations will aid in optimizing individualized protocols for clinical applications.

Purpose: To determine the effective dose for a range of imaging protocols using the Sirona GALILEOS Comfort CBCT scanner.

Materials and Methods: Calibrated InLight nanoDot OSL dosimeters (Landauer, Glenwood, Ill) were placed at 26 select sites in the head and neck of a modified, human tissue-equivalent RANDO phantom. Effective dose was calculated using the measured local absorbed doses, accounting for the fractional volume and type of tissue exposed, and applying the 2007 ICRP¹ tissue weighting factors. In total, 12 different scanning protocols were investigated varying the field of view, mAs, contrast and resolution parameters.

Results: The effective doses for a repeated protocol (full maxillomandibular scan, maximum (42) mAs, high contrast and resolution) were 140, 141 and 142 μ Sv. This compares to 100 μ Sv for a maxillary scan and 107 μ Sv for a mandibular scan with identical mAs, contrast and resolution settings. Effective dose remained between 140-142 μ Sv for maxillomandibular scans at 42 mAs with varying contrast and resolution settings.

Conclusions: Changes to mAs and beam collimation have a significant influence on effective dose. Effective dose varies linearly with mAs. Collimating to obtain a narrower maxillary or mandibular scan decreases effective dose by approximately 28% and 23% respectively as compared to a full maxillomandibular scan. Changes to contrast and resolution settings have little influence on effective dose. This study provides data for setting individualized patient exposure protocols in order to minimize patient dose from ionizing radiation used for diagnostic or treatment planning tasks in dentistry

Keywords: *dosimetry, radiation dosage, effective dose, cone beam computed tomography, CBCT*

Co-Authorship Statement

This study was the result of a collaborative effort among several individuals. Completion of this thesis was not possible without their important contributions.

David Chambers – wrote thesis, study design, data collection and analysis

Dr. Richard N. Bohay – supervisor, reviewed thesis, study design and analysis

Dr. Jerry Battista (Biophysics) – advisor, study design and analysis, thesis editing

Linada Kaci (Biophysics) – reviewed thesis, study design, data collection and error analysis, dose calibration of OSL dosimeters

Dr. Rob Barnett (Biophysics) – study design and analysis, provided access to dosimetry equipment and calibration x-ray beam of the London Regional Cancer Program, London Health Sciences Centre

Acknowledgments

I would like to express my sincere appreciation to all of those who made important contributions in completing this project.

I wish to thank my co-supervisors Dr. Richard Bohay and Dr. Jerry Battista. Your enthusiasm, insight and genuine interest made for a positive research experience. I was fortunate to receive your combined guidance.

This project would not have been possible without the valuable assistance of Linada Kaci. Her willingness to provide much of her time despite many clinic responsibilities was greatly appreciated. I could not have asked for a better research partner.

A very special thank you to Dr. Antonios Mamandras, Dr. Ali Tassi, Dr. John Murray and Dr. Jeff Dixon for recognizing my desire to study this specialty and extending me that privilege. I will always be grateful.

Thank you to all of the full-time and part-time faculty members for your dedication to this profession in providing your time to enhance my professional and academic development. To Jo Ann Pfaff, Barb Merner, Evelyn Larios, Patricia Vanin and Jacquie Geneau, thank you for all your continued assistance and support, the clinic is fortunate to have such a great team.

To my fellow residents, past and current, I was fortunate to spend my time with such an amazing group of individuals. To my classmates Natalie Swoboda and Bhavana Sawhney, thanks for the laughs and continued encouragement. I am grateful for the opportunity to have shared this experience with you.

Finally, a sincere thank you to my parents and loved ones for your continued support in realizing my academic goals. Accomplishing them was a direct result of your influence and encouragement.

Table of Contents

Abstract.....	ii
Co-Authorship Statement.....	iii
Acknowledgments.....	iv
Table of Contents.....	v
List of Tables.....	vii
List of Figures.....	viii
List of Appendices.....	ix
List of Abbreviations.....	x
INTRODUCTION.....	1
BACKGROUND.....	3
X-Radiation.....	3
Dental Radiology: History.....	3
Development.....	3
Dental Radiographic Techniques.....	4
The Biologic Effects of Radiation.....	11
Radiation Dosimetry.....	12
Exposure.....	12
Absorbed Dose.....	12
Equivalent Dose.....	13
Effective Dose.....	14
Experimental Dosimetry Methods.....	15
Dosimeters.....	16
CBCT Protocol Parameters.....	18
Field of View.....	18

Scan Time	18
Exposure Time	19
CBCT Voxel Size	19
Sirona GALILEOS® Parameters	19
PURPOSE	21
MATERIALS AND METHODS	22
Dosimeters	22
Phantom	23
Anatomic Landmarks	25
Phantom Orientation	27
Protocols	29
RESULTS	32
DISCUSSION	36
SUMMARY	42
CONCLUSIONS	43
REFERENCES	44
APPENDICES	50
CURRICULUM VITAE	56

List of Tables

Table 1: Effective dose estimates for common dental radiographs	10
Table 2: Radiation weighting factors recommended by ICRP	13
Table 3: Tissue weighting factors as recommended by ICRP (2007)	14
Table 4: Comparison of TLD and OSLD properties	17
Table 5: Anatomic sites for dosimeter placement.....	25
Table 6: Summary of protocols investigated	29
Table 7: Percentage tissue irradiated, tissue weighting factor and OSLD sample for each tissue/organ	31
Table 8: Effective dose calculations for protocols completed.....	32
Table 9: Effective dose of collimated scans	33
Table 10: Equivalent dose (μSv) to tissues/organs.....	34
Table 11: Equivalent doses for maxillary scan as a percentage of equivalent doses for mandibular scan (taken as mean of percentages for 14, 28 and 42 mAs).....	34
Table 12: Effect of resolution and contrast on dose	35

List of Figures

Figure 1: Sample Image, Sirona GALILEOS®	8
Figure 2: Available Exposure Settings for GALILEOS® Comfort.....	19
Figure 3: Therapax HF 150.....	23
Figure 4: PMMA template for OSLD placement	24
Figure 5: RANDO® phantom with PMMA templates in place	24
Figure 6: Relationship of hard and soft tissue in RANDO® phantom	26
Figure 7: Lateral Cephalometric view with lead foil at OSLD locations	27
Figure 8: Modified mount for setup reproduction	28
Figure 9: 'Tilt' and 'Rotation', confirming setup reproduced.....	28
Figure 10: High intensity light source to anneal OSL dosimeters	30
Figure 11: Effective Dose vs mAs	33

List of Appendices

Appendix A: Average OSLD Counts - Full Scan, 42mAs, HC/HR	51
Appendix B: Average OSLD Counts - Full Scan, HC/HR	52
Appendix C: Average OSLD Counts - Maxillary Scan, HC/HR.....	53
Appendix D: Average OSLD Counts – Mandibular Scans, HC/HR	54
Appendix E: Average OSLD Counts – Full Scans	55

List of Abbreviations

ALARA	As Low as Reasonably Achievable
CBCT	Cone Beam Computed Tomography
CCD	Charge Coupled Device
CMOS	Complementary Metal Oxide Semiconductors
CT	Computed Tomography
CTDI _{vol}	Computed Tomography Dose Index by Volume, accounting for overlap of CT slices
CTDI _w	Weighted Computed Tomography Dose Index, averaging dose in a CT slice
D _T	Absorbed Dose for tissue 'T'
E	Effective Dose – in units of Sievert (see below), a weighted sum of tissue/organ doses (D _T)
EBM	Electronic Band Model
FOV	Field of View
Gy	Gray (unit of Absorbed Dose – 1 J/kg)
HC	High Contrast
HR	High Resolution
H _T	Equivalent Dose for tissue 'T'
HVL	Half Value Layer (requirement to attenuate 50% of incident radiation)
ICRP	International Commission on Radiological Protection

keV	kiloelectronvolts
kV	kilovoltage
LET	Linear Energy Transfer
mA	milliampere (x-ray tube current)
mAs	milliampere seconds (product of mA and time)
MDCT	Multidetector Computed Tomography
MeV	Megaelectronvolts
MV	Megavolts
NC	Normal Contrast
OSLD	Optically Stimulated Luminescence Dosimeter
P_{KA}	Air Kerma-Area Product
$P_{KL,CT}$	CT Air Kerma-Length Product
PMMA	Polymethyl methacrylate
PSP	Photostimulable Phosphor
R	Roentgen (unit of radiation exposure)
SR	Standard Resolution
Sv	Sievert (unit of Effective Dose)
TAD	Temporary Anchorage Device
TLD	Thermoluminescence Dosimeter
TMJ	Temporomandibular Joint

VO1	Volume 1 (High Resolution)
VO2	Volume 2 (Standard Resolution)
W_R	Radiation Weighting Factor for radiation type 'R'

INTRODUCTION

Dental radiography provides essential information in diagnosis and subsequent treatment planning. While two-dimensional analog techniques continue to be employed in routine dental practice, digital and three-dimensional modalities are becoming increasingly common. Digital radiography offers improved compatibility with practice management and imaging software, reduces storage needs, eliminates chemical, Silver and lead foil waste, facilitates transfer of images between practitioners and may offer reduced radiation exposure.² Three-dimensional imaging techniques provide a means for interpreting the spatial relationship of structures otherwise superimposed on standard two-dimensional images. This has important implications in dental implantology and other surgical procedures where detailed assessment of structures adjacent to the surgical site is essential. In clinical situations where several two-dimensional images are indicated, three-dimensional techniques offer an efficient method of reconstructing the same group of images while limiting image acquisition to a single exposure.³

While three-dimensional images may offer abundant clinical information, it is not sufficient to prescribe them on the basis of convenience. Of equal importance in determining which image to prescribe is the associated radiation exposure incurred by the patient. Haphazard selection of images that exceed the region of interest and quality required for diagnosis exposes the patient to undue risk from ionizing radiation. For this reason, guidelines suggest that radiation exposure be limited to as low as reasonably achievable, with the benefits from the diagnostic information obtained exceeding the risks incurred by exposure.⁴⁻⁶

The question of which radiograph to prescribe for a given patient and clinical scenario becomes a complex one requiring an in depth knowledge of the parameters set at image acquisition and their respective effects on both diagnostic image quality and patient exposure. Obtaining an image with maximum field and resolution may provide the most complete set of imaging data for the patient but at the expense of increased radiation dose. Determination of the appropriate scanning protocol must be considered in the context of the patient history, clinical findings, previous imaging results, differential diagnosis and treatment plan. The scanning protocol must also take into consideration the age and size of the patient as well as the ability of the scan to demonstrate the anatomy of interest. It becomes obvious that image protocol optimization is not

a simple task and prescription requires a thorough knowledge of both diagnostic imaging and the risks of biologic effects due to ionizing radiation.

The purpose of this study is to investigate the effective radiation dose associated with the Sirona GALILEOS® Comfort Cone Beam CT scanner using different scanning protocols. An understanding of the effect of field of view (FOV), milliamperere seconds (mAs), contrast and resolution (voxel size) on effective dose will aid the clinician in determining the optimum protocol for each patient and clinical question. This study will focus on exposure while it is understood that image quality is also of importance and will require subsequent study.

BACKGROUND

X-Radiation

The x-ray was discovered in 1895 by Bavarian physicist Wilhelm Roentgen.⁷ Roentgen was experimenting with cathode rays using a vacuum tube, electrical current and screens that fluoresced when exposed to radiation when he noticed that screens on an adjacent table were fluorescing. The screens were several feet away from the vacuum tube, a distance greater than cathode rays could travel. He therefore concluded that there existed an unknown ray responsible for these findings and named it the x-ray due to its unknown properties. Roentgen continued to experiment with x-rays eventually obtaining the first radiograph of the human body, that of his wife's hand.⁷

Dental Radiology: History

Development

With the discovery of the x-ray came interest in dental imaging. In 1895 German dentist Otto Walkhoff obtained the first dental radiograph of his own mouth.⁷ Continued experimentation by several pioneers lead to application on live patients and the development of radiographic techniques. Boston dentist William Rollins is accredited with the development of the first dental x-ray unit.⁷ He introduced interest in radiation protection recognizing the dangers of radiation. Unfortunately early pioneers were not aware of the associated dangers with many suffering the effects of overexposure to radiation.

In 1913, William Coolidge developed the first hot-cathode x-ray tube. It consisted of a high-vacuum tube with a tungsten filament and serves as the prototype for all modern x-ray tubes. Victory X-Ray Corp. began manufacturing an x-ray machine with a small version of the x-ray tube within the head in 1923. This design was later superseded by the variable kilovoltage machine in 1957 with introduction of the recessed long-beam tube head in 1966.⁷

Initial dental x-ray packets were fabricated from glass photographic plates, wrapped in black paper and rubber. Eastman Kodak Company began manufacturing pre-wrapped intraoral film in 1913 with the first periapical packets available in 1920. Subsequent improvements in film lead

to D-speed film in 1955, E-speed film in 1981 and F-speed film in 2000. Current fast film requires less than 2% of the exposure required for that available in 1920.

The modern era of digital dental radiography followed Dr. Francis Mouyen's 1989 paper describing radiovisiography.^{8,9} Multiple advantages have resulted in a shift toward digital imaging in dentistry including lower patient exposure, ability to transfer images between health care providers without degradation in image quality and a reduction in chemical, Silver and lead foil waste associated with analog imaging.² Two main technologies exist, solid-state technology and photostimulable phosphor (PSP) technology.² Solid state detectors function by collecting the charge produced by x-rays in a solid semiconducting material producing rapid image availability.² Subtypes include charge-coupled devices (CCD), complementary metal oxide semiconductors (CMOS) and flat panel detectors. Photostimulable phosphor plates absorb energy from x-rays. Stimulation by appropriate light leads to release of this energy in the form of visible light and subsequently quantified to measure the amount of x-ray energy absorbed.

Dental Radiographic Techniques

Intraoral

Soon after the discovery of x-rays, dental radiographic techniques began to emerge. Edmund Kells of New Orleans, with many significant contributions to radiology in North America, introduced the paralleling technique in 1896 while Weston Price introduced the bisecting technique in 1904. This was later refined by Howard Raper when introducing the bite-wing technique in 1925.⁷ Franklin McCormack began use of the paralleling technique in 1920 and in 1937 published a paper explaining the advantages to the long distance paralleling technique in minimizing distortion when compared to the bisecting technique.^{7,10} These advantages were realized when F. Gordon Fitzgerald introduced the long-cone paralleling technique in 1947.

Extraoral

Cephalometry

Craniometry is described as the art of measuring the skulls of animals and has been documented for many centuries.¹¹ It provided the foundation for cephalometry which involves measuring the head inclusive of soft tissue. Documentation of skull form analysis dates back to Hippocrates

(460-357BC).¹¹ Leonardo da Vinci (1452-1519) was one of earliest to apply the theory of head measurement, using a variety of lines relating to head landmarks in order to study human form.¹¹ Craniometry continued to develop in the following centuries during which the craniostat was developed in recognizing the importance of reproducibility and standardized methods.¹¹

In 1922, A.J. Pacini published a thesis entitled “Roentgen Ray Anthropometry of the Skull” in which he outlined a procedure for positioning and immobilizing a subjects head such that the median sagittal plane was parallel to the film.^{12,13} This was developed for anthropologic purposes. It was not until 1931 that dentists Hofrath and Broadbent simultaneously published details on an apparatus, the ‘cephalostat’, used to position the heads of live patients in relation to the x-ray source and film such that the lateral cephalogram could be obtained.¹¹ Subsequently, the art and science of cephalometrics developed gaining widespread acceptance for use in diagnosis, study of growth and development and the effects of treatment.¹³

Conventional Tomography:

Clinical demand for three-dimensional imaging lead to the development of conventional tomography with Polish radiologist Mayer first suggesting the idea in 1914.¹⁴ This technique is used to obtain an image of a select plane of tissue while blurring adjacent structures.⁷ In conventional film-based tomography, the x-ray tube and film are rigidly connected and synchronous movement around a fixed axis produces a sharp image layer (‘tomographic layer’) with adjacent structures outside the focal plane blurred.² Several types of movement are possible including linear, circular, elliptic, hypocycloidal and spiral.²

Panoramic

While much utility was recognized in early intraoral techniques, the need for obtaining an unobstructed view of the maxilla, mandible and dentition was recognized. In 1922, A.F. Zulauf patented the ‘panoramic x-ray apparatus’, describing a method where a narrow beam scanned both the upper and lower jaws.^{15,16} Hisatugu Numata of Japan was the first to expose a panoramic radiograph in 1933, using a device constructed for clinical examination termed “parabolic radiography” with the film placed lingual to the dentition.¹⁵ Yrjo Paatero of Finland, considered the ‘father of panoramic radiography’ experimented with slit beam and rotational

techniques. He published several papers describing use of the technique in clinical practice.^{7,15,17-20}

Development of commercial equipment for panoramic radiography began with production of the Orthopantomograph by Palomex under the charge of Timo Nieminen in 1960.¹⁵ Increased clinical use resulted in progression to large-scale production. Early models of commercial equipment were controlled by mechanical means. The first publication on computed panoramic radiography was released by H. Kashima et al of Japan in 1985 with the first electronic system for rotational panoramic radiography reported by McDavid et al in 1991.²¹⁻²³

Conventional Computed Tomography (CT)

Computed tomography has undergone continued development since first introduced for clinical application. Related theory dates back to 1917 when mathematician J.H. Radon proved the distribution of an x-ray attenuating material in an object layer can be calculated if the integral values along many ray-lines passing through the same layer are known.²⁴ The Radon transform provided the mathematical basis for image reconstruction from data associated with cross-sectional scans.²⁴ Physicist A.M. Cormack developed the first medical applications.²⁴ From 1957-1963 he developed a method of calculating radiation absorption distributions in the human body based on transmission measurements. With these findings, Cormack proposed it was possible to display small absorption differences which would have application in imaging of soft tissues for planning radiation treatment of cancer.

In 1972 English engineer G.N. Hounsfield found practical application for theory relating to tomography when he designed the first practical Computed Tomography (CT) scanner.²⁴ He conducted the first clinical examinations with J. Ambrose in 1973 at British firm EMI. Sixty EMI scanners were installed by 1974 with 18 companies offering CT equipment and more than 10,000 devices in use by 1980.²⁴ In recognition of their significant work, Hounsfield and Cormack were both awarded the Nobel Prize for medicine in 1979.²⁴

The first-generation CT unit introduced in 1971 by EMI limited exposure to one pencil beam at a time, the x-ray source collimated to a beam measuring 3mm wide by 13mm long. The x-ray source and detector both translated linearly to collect 160 measurements across the field after

which the tube and detector rotated one degree before collecting the subsequent set of measurements.²⁵ The method of data collection resulted in limited efficiency in scan time, each scan taking approximately 4.5 minutes. Image quality was therefore compromised as a result of patient motion.

The second-generation CT scanner was developed with the intent of reducing total scan time and thus the effects of patient motion on image quality. This was accomplished by introducing multiple (six) adjacent tilted pencil beams, each with an angle differing by one degree. With this design, a scanner could translate across the patient but rotate at six degree intervals between sets of measurements. In 1975 EMI introduced a scanner with 30 detectors capable of a complete slice scan in under 20 seconds, thus within the range of holdings one's breath.²⁵

Further efficiency was accomplished in developing the third-generation CT scanner. This design utilizes a broad fan shaped beam with many more detector cells arranged on an arc concentric to the source. Unlike the previous generations, the source and detector remain coupled to each other as they rotate around the patient. With such a design, the width of the entire object slice is irradiated by the source at any given time and no linear motion is required, ultimately reducing data acquisition time. The third-generation scanner accounts for most modern scanners on the market today.²⁵

The fourth-generation scanner is designed using a stationary detector formed as a closed ring. The x-ray tube rotates around the patient with signals measured on a single detector at a given time. A fan shaped beam is formed, however the apex is located at the detector rather than the source as found in the third-generation. With this method each detector cell can be exposed to the x-ray source without attenuation at some point in the scan thus allowing for detector recalibration. This method however requires a very large number of detectors and there is no practical method for post-patient collimation. This requires an increased acceptance of scattered radiation and hence poorer contrast. This design is less practical than the third-generation and it is for this reason the third-generation remains the dominant design in current clinical application.²⁵

Cone Beam Computed Tomography (CBCT)

Cone-beam computed tomography (CBCT) was introduced to the U.S. market in 2001 with the NewTom QR DVT 9000.^{3,26} In 2005 there were 4 main CBCT scanners reported in the literature with over 45 scanners offered by 20 manufacturers reported at the time of this writing.²⁷ An overview of these scanners including technical specifications was provided by Nemtoi et al.²⁷ This growth in manufacturers has resulted from continued development and application of CBCT in both dentistry and general medical radiology.

With CBCT, a diverging x-ray beam is limited by a circular or rectangular collimator to match the corresponding 'flat panel' detector or region of interest. The conic source and detector rotate as a unit around the patient up to 360 degrees. While rotating, a sequence of multiple two-dimensional radiographic images is obtained. 'Back projection' of all image data results in a 3D array of three-dimensional volume elements referred to as 'voxels', which in general range in size from 0.07 to 0.40mm³. Software is used to reconstruct and display this three-dimensional volume (Figure 1).²⁶



Figure 1: Sample Image, Sirona GALILEOS®

<http://www.sirona.com/en/products/imaging-systems/GALILEOS®>

Tissues and space within the region of interest vary in their x-ray attenuation values and voxels corresponding to their location are assigned relative gray-scale values. Current units are capable of producing between approximately 4000 and 16,000 shades of gray. Since current computer monitors produce 256 shades of gray, software is used to overcome hardware limitations through use of 'windowing' and 'leveling' functions. These functions allow the user to visualize 256 shades of gray at a time distributed around the tissue attenuation values of interest. After leveling is optimized for the tissues of interest, windowing is adjusted for contrast in a narrow band of attenuation values centred about the level value.²⁶

CBCT Applications

Cone beam CT has applications in numerous branches of health care including angiography, surgical planning and intraoperative imaging, neuroradiology, image guided radiation therapy, otolaryngology and dentistry.²⁸ Applications for CBCT imaging in dentistry and orthodontics have continued to increase since introduction to the market. In orthodontics applications include but are not limited to the three-dimensional assessment of impacted and ectopically erupting teeth, TMJ analysis, airway assessment, study of growth and development and treatment planning. Suggested benefits in treatment planning include improved accuracy in cephalometric landmark identification and soft tissue profile, optimal assessment of location for Temporary Anchorage Device (TAD) placement and improved orthognathic surgery planning.²⁹

Despite the reported benefits from manufacturers and practitioners, further evidence is required to justify the added burden of radiation exposure. A systematic review conducted by van Vlijmen et al²⁹ investigated the applications of CBCT imaging in orthodontics, evaluating the respective levels of evidence. The authors identified 550 articles describing application in the use of TADs, cephalometry, combined orthodontic and surgical treatment, airway analysis, root resorption, tooth impactions and cleft lip and palate treatment. Fifty articles met inclusion criteria. No high-quality evidence was identified to support a significant benefit of CBCT use in orthodontics with only airway diagnoses suggesting improved value in comparison to two-dimensional imaging techniques.²⁹

While it is difficult to justify the routine use of CBCT imaging in dentistry and orthodontics, when three-dimensional imaging techniques are indicated CBCT techniques offer several advantages when compared to conventional CT scans of the head. The most important advantage is a large reduction in patient dose.³ The reported effective dose of small and medium FOV units is 11-674 μ Sv (median 61 μ Sv) with large FOV units ranging from 30-1073 μ Sv (median 87 μ Sv).⁶ Reported effective dose from conventional CT is significantly higher, ranging from 1,320-3,324 μ Sv for a mandibular scan and 1,031-1,420 μ Sv for a maxillary scan.⁶ While CBCT doses are lower than standard CT doses, they are still significantly higher than other dental radiographic procedures. Table 1 summarizes the effective dose associated with common two-dimensional radiographic techniques.⁶ The average background dose for all people on earth is approximately 2400 μ Sv per year, or 6.6 μ Sv per day.³⁰

<i>Imaging Technique</i>	<i>Effective Dose (μSv)</i>
Four posterior bitewings (digital PSP or F-speed film & rectangular collimation)	5
Panoramic radiograph with charge-coupled device	3.0-24.3
Cephalometric radiograph with PSP	5.1-5.6
Full-mouth radiographs:	
PSP or F-speed film and rectangular collimation	34.9
PSP or F-speed film and round collimation	170.7

Table 1: Effective dose estimates for common dental radiographs⁶

Cone-beam CT offers several non-dosimetric advantages when compared to conventional CT. Reduced size and cost increases clinical practicality outside the hospital setting. The field of view (FOV) can often be reduced when desired with resulting reduction in exposure. Other advantages include a reduction in scan time comparable to spiral MDCT minimizing effects of patient motion, reduction in metal artifacts as a result of algorithms designed by the manufacturer and display modes unique to maxillofacial imaging.³

The Biologic Effects of Radiation

The biologic damage associated with radiation exposure is thought to be due to the direct action of radiation on DNA as well as the indirect action of free radicals produced in water. Interaction of radiation with water produces free oxygen radicals that interact with other molecules causing damage to cell structures including DNA.³¹

In humans, the biologic effects of radiation can be categorized as stochastic (i.e. random) or nonstochastic (i.e. non-random). Nonstochastic effects were previously referred to as acute effects and in current terms ‘deterministic effects’.³¹ Deterministic effects are characterized by a threshold below which effects are not observed. When the threshold is exceeded, the effects are seen and the magnitude increases with increased dose. Such effects show a clear association with radiation exposure.³¹ Examples include erythema, loss of hair, cataracts, nausea, vomiting and depression of bone marrow cell division.³¹

Stochastic effects were previously referred to as “late effects” as they usually occur years after exposure. Certain tissues are at higher risk for stochastic effects, in particular those composed of cells with a high division rate, long dividing future and/or unspecialized type such as progenitor cells found in bone marrow.³¹ Such effects may or may not present in a given individual and are thus probabilistic in nature.³¹ The probability of stochastic effects increases with radiation dose but not necessarily the magnitude of the effect. In contrast to nonstochastic effects, a threshold may not exist and there lacks a clear association between exposure and effect. Examples of stochastic effects include cancer and hereditary effects on the offspring of exposed individuals.³¹

In oral and maxillofacial diagnostic imaging the primary concern is the risk for stochastic effects, namely radiation induced cancer.² This is because the doses given are all well below the thresholds for deterministic effects. Recognizing the risk associated with radiation exposure, prescription of dental and medical imaging must be done with diligence. Dosimetry studies provide a means of estimating the biologic risk associated with radiation used in imaging or therapy. Radiation dosimetry is the focus of this work.

Radiation Dosimetry

Interaction of radiation with matter results in a transfer of energy to the atoms constituting tissue.³¹ Dosimetry is the determination of dose or the quantity of radiation exposure.² Dose is described in terms of the energy absorbed per unit mass at a site of interest. In clinical context, dosimetry ultimately provides estimates of the biologic effects of radiation from which appropriate therapeutic and diagnostic use can be determined. Several methods are used to measure the quantitative effects of ionizing radiation with matter.

Exposure

When ionizing radiation interacts with matter ions are produced which have a net charge. Counting the resulting ions formed in air is the simplest method for measuring the quantitative effects of ionizing radiation. This can be accomplished by using oppositely charged surfaces to attract and count the ions formed. The quantity exposure is a measure of radiation based on the ability to produce ionization in air under standard temperature and pressure conditions. It provides a measure of the radiation present in an environment and is useful in survey meter measurements.³¹ Air kerma ('kinetic energy released in matter') is the SI unit of exposure and is expressed in units of dose, Gray [Gy= 1 Joule/kg] replacing the traditional unit of Roentgen (R).²

Absorbed Dose

While exposure provides a measure of the radiation present in the environment, it is of greater clinical importance to know the quantity of radiation actually absorbed by patients. The 'absorbed dose' describes the energy absorbed from any type of ionizing radiation per unit mass of any type of matter.^{2,31}

The SI unit for absorbed dose is also the Gy replacing the traditional unit of 'rad' ('radiation absorbed dose') which is equal to 1cGy.² The absorbed dose is thus determined by the following equation:

$$\text{Absorbed Dose } D = \frac{\text{energy absorbed from ionizing radiation}}{\text{mass}} = \frac{d\varepsilon}{dm}$$

Equivalent Dose

Absorbed dose measures the physical energy absorbed but does not account for the fact that different types of radiation have a different potential in producing biological damage. High linear energy transfer (LET) radiations such as high-energy protons are more damaging to tissue than lower LET radiations such as x-rays.³¹ The radiation weighting factor (W_R) accounts for this relative biologic effect in human tissue and provides the basis for calculating the equivalent dose (H_T). The radiation weighting factor is dimensionless and therefore equivalent dose is represented in the same units as absorbed dose but may be described in the special unit of Sieverts (Sv). The corresponding definitions are as follows:

$$\text{Equivalent Dose } H_T = \text{Absorbed Dose } D_T \times \text{Rad. Weighting Factor } (W_R)$$

$$\text{Equivalent Dose } Sv = \text{Dose } Gy \times W_R$$

The current radiation weighting factors as determined by the International Commission on Radiological Protection (ICRP) are summarized in Table 2.

Type of Radiation	W_R
Photons	1
Electrons and muons	1
Neutrons, energy:	
< 10 keV	5
10 – 100 keV	10
> 100 keV to 2MeV	20
> 2 MeV to 20 MeV	10
> 20 MeV	5
Protons, other than recoil protons, $E > 2$ MeV	5
Alpha particles, fission fragments, heavy nuclei	20

Table 2: Radiation weighting factors recommended by ICRP¹

For the x-rays used in dental CBCT, the radiation weighting factor is 1.0; hence the values of Dose (in Gray) matches the values of Equivalent Dose (in Sv).

Effective Dose

When an individual is exposed to radiation it may be to the whole body or in part. Reducing the proportion of tissues exposed to radiation reduces the potential for biologic damage. In addition, tissues differ in their radiosensitivity and risk for stochastic effects including cancer formation.² Effective dose (E) provides a means of estimating the biologic risk in humans exposed to radiation. It allows for comparison of risk between partial exposures by representing such exposure as a full-body dose of equivalent detriment.² Each tissue is assigned a tissue-weighting factor (W_T) (Table 3). The effective dose is measured in units of Sieverts (Sv) and obtained through the sum of the products of average equivalent dose to each tissue and the associated tissue weighting factor. This is summarized as follows:

$$\text{Effective Dose } E = \sum W_T \times H_T$$

<i>Organ</i>	<i>Tissue Weighting Factor (W_T)</i>
Gonads	0.08
Red bone marrow	0.12
Colon	0.12
Lung	0.12
Stomach	0.12
Bladder	0.04
Breast	0.12
Liver	0.04
Oesophagus	0.04
Thyroid	0.04
Skin	0.01
Bone surface	0.01
Brain	0.01
Salivary Glands	0.01
Remainder	0.12

Table 3: Tissue weighting factors as recommended by ICRP (2007)¹

It is important to note that this assumes exposure to the full tissue volume. If a given tissue is only exposed in part, it must also be taken into consideration when calculating the effective dose.

For example, in diagnostic radiology an image may only expose a fraction of the body's skin. The relative proportion of skin exposed is taken into consideration by multiplying the fraction exposed by the skin's contribution to effective dose as follows:

$$f_{skin} \times W_{skin} \times H_{skin}$$

Experimental Dosimetry Methods

There are several methods available for estimating the effective dose imparted by ionizing radiation all of which rely on computations or measurements in patient-like 'phantoms' and present with some limitations.³² The most common methods include organ dose, computed tomography dose index by volume (CTDI_{vol}), CT air kerma-length product (P_{KL,CT}), Air kerma-area product (P_{KA}), Monte Carlo dose simulation programs, entrance surface skin dose and energy imparted. Organ dose measurements or calculations using and Monte Carlo simulations are common techniques employed in dental CBCT studies while CTDI_{vol} measurement is most common in conventional CT dosimetry studies and warrants discussion.

The computed tomography dose index by volume (CTDI_{vol}) represents the mean absorbed dose in the examination volume.³² A 100mm pencil ionization chamber is used to measure the kerma-length product (P_{KL}) at the centre and periphery of standardized cylindrical phantoms with dimensions representing the head or body. The weighted CTDI (CTDI_W) is the sum of one-third of the value at the centre and two-thirds of the value at the periphery, corresponding to the average dose in a slice, assuming abutted but non-overlapping slices. The CTDI_{vol} is obtained by dividing the CTDI_W by the pitch used for examination to account for overlapping slices using helical scanning.³² While this method has proven effective for single slice CT scanners with slice thicknesses not exceeding 10mm, several studies have demonstrated limited applications to thicker beam widths used in CBCT.^{33,34} As such, CTDI_{vol} may present with limitations in characterizing the dose associated with CBCT images.

Organ dose is based on estimates of the mean absorbed dose to different organs and tissues using dosimeters placed locally within a human anthropomorphic phantom.³² These phantoms are often composed of a natural human skeleton contained within a material radiologically equivalent to human soft tissue. Accuracy in determining mean organ dose is limited given the

finite and limited number of dosimeters used. Effective dose is obtained using the mean tissue doses and tissue weighting factors established by the ICRP.¹ This method is the most predominant in studies relating to CBCT dosimetry in dentistry.

Estimates of effective dose can also be obtained by mathematical models including Monte Carlo simulations.³² This technique uses knowledge of exposure parameters and beam quality together with a mathematical phantom of attenuation values to obtain an effective dose based on simulation of individual particle interactions and trajectories.³²

Dosimeters

Organ dose measurement is the most common dosimetry method found in dental CBCT studies. The mean organ or tissue dose is determined by measuring the absorbed dose at a select number of sites within a given organ or tissue. This is accomplished by use of dosimeters.

Thermoluminescent (TL) dosimeters are historically the most common used in dental CBCT studies while newer optically stimulated luminescent (OSL) dosimeters are likely to become more common as they have proven accurate while offering efficient readouts with the option of being stored and reread at a later time.

Luminescence describes a process by which energy absorbed by a semiconductor or insulator from ionizing radiation is subsequently released in the form of light (electromagnetic radiation) upon exposure to heat (thermoluminescence, TLD) or light (optically stimulated luminescence, OSL).³⁵ This phenomenon is very useful in radiation dosimetry since the quantity of light emitted is proportional to the radiation dose absorbed by the material.³⁵

Many general models have been proposed to explain the mechanism of luminescence in select materials, one of which is the electronic band model (EBM).³⁵ The theory suggests the presence of an energy band gap, or “forbidden band” separating two different energy bands, the valence and conduction bands. Exposure to ionizing radiation results in excitation of electrons to the conduction band with resulting holes in the valence band. These electrons and holes move within the material until they recombine or are captured by localized intermediate energy levels acting as traps. The trapped charges can be stimulated back to the conduction band with subsequent de-excitation resulting in electron-hole recombination with resulting luminescence.

The intensity of luminescence is related to the trapped charge concentration and thus absorbed dose.³⁶

For personal dosimetry, LiF:Mg,Ti (TLD-100) are the most common TL dosimeters used while other suitable materials include LiF:Mg,Cu,P, CaSO₄:Dy and ZrO₂.³⁵ Another material originally developed as a sensitive TLD material is Al₂O₃:C but its sensitivity to daylight instead resulted in the research leading to OSL development.³⁷ Additional materials that followed for OSL include BeO, MgO, ABF fluorides, Ammonium salts and alkali halides.³⁷ While thermoluminescent dosimeters have been used successfully for many decades, use of OSL dosimeters has become increasingly popular. Table 4 summarizes the characteristics of both TL and OSL dosimeters.

	<i>TLD</i>	<i>OSLD</i>
Accuracy	High (uncertainty ~3% for high doses) ³⁵	High ³⁵ (uncertainty 0.7-3.2%) ³⁶
Precision	High ³⁵ (reproducibility ~1.5%) ³⁸	High ³⁵ (reproducibility <1%) ³⁸
Dose Linearity	Supralinear >10Gy ³⁹	Supralinear >3Gy ⁴⁰
Reuse	Reuseable ³⁵	Reuseable ³⁸
Energy Dependence	Correction Factor Required ⁴¹	Correction Factor Required ⁴¹
Tissue Equivalence	Tissue equivalent ³⁵	Nearly equivalent ³⁷
Size	~ 3x3x1mm ³⁸	~ 7x7x0.5mm ³⁸
Directional Dependence	None ³⁵	3-4% ⁴² None ³⁸
Temperature Dependence	Independent at ambient temperature ³⁵	Independent ³⁸
Fading	Subject to fading ³⁵	Wait time of 8min Slow fading day 17-38 ^{38,43}
Readout Time	No instant readout ³⁵ Technique sensitive	~ 8 min wait ³⁸ ~1min to read

Table 4: Comparison of TLD and OSLD properties

CBCT Protocol Parameters

When a radiological examination is required an imaging protocol is established. A protocol is a set of exposure parameters (kV, mAs, FOV) defined by the clinician and developed to produce images of optimal quality while minimizing radiation burden to the patient.² While standard protocols are often pre-programmed by CBCT manufacturers, parameters may be modified by the radiologist. Scan parameters usually include scanning volume (field of view), voxel size (/resolution), the number of basis projections and exposure time.²

Clinical guidelines suggest that radiation dose be optimized in accordance with the ALARA principle. The principle states that dose should be restricted to as low as reasonably achievable.⁶ To accomplish this, the image should be restricted to a narrow field of view and produce image quality sufficient to answer the clinical question being addressed. The quality of the image is dependent on multiple parameters such as desired spatial and contrast resolution determined by the clinician prior to exposure. An understanding of the effects of these parameters on both image quality and dose is necessary to achieve an optimized protocol for each individual patient and associated clinical question.

Field of View

Field of View (FOV) is established by collimating the primary x-ray beam, limiting x-radiation to the region of interest thereby reducing effective dose by exposing only a subset of tissues and organs.² Maximum field of view differs between CBCT units on the market, with small FOV machines beginning at 3x4x4mm (3D Accuitomo) and large FOV machines up to 20x20x20 cm (NewTom 3G).⁴⁴ Many units offer multiple FOV settings which may for example be suitable for mandibular, maxillary or maxillofacial scans. Restricting the field of view to the region of interest effectively reduces radiation dose and improves images quality by reducing scatter radiation.²

Scan Time

A CBCT scan is composed of a series of basis radiographic image projections. In theory, a perfect reconstruction is possible if an infinite number of two-dimensional projections are obtained at an infinite number of angles. This of course is not practical and instead a finite

number of basis images is selected by adjusting the frame rate while the x-ray tube rotates.² Increasing the number of basis projections increases image quality but patient exposure increases proportionately.²

Exposure Time

For optimal image quality the radiographic projections measured at the detector must be neither underexposed nor overexposed. This number of x-rays at the imaging detector is determined by the number of x-rays produced, a product of milliamperage (mA) and exposure time (s).² An increase in milliampere-seconds (mAs) may improve image quality but at the expense of increased patient radiation exposure. An optimum image protocol will establish an exposure time for which image quality is diagnostic but patient exposure minimized.

CBCT Voxel Size

The voxel size varies between manufacturers with individual units often allowing user selection of voxel size. A decrease in voxel size increases spatial resolution but results in increased radiation exposure for a fixed noise level.²

Sirona GALILEOS® Parameters

With the Sirona GALILEOS® CBCT scanner, the tube voltage is fixed at 85kV, with a current of 7mA (reduced to 5mA for 10mAs setting) and number of basis images (i.e. projections) is set at 200 by the manufacturer. The user can establish multiple protocols by varying the mAs, field of view (FOV) and using high contrast or high resolution modes (voxel size 0.15 – 0.3mm). The mAs options include 10, 14, 21, 28, 35 and 42 mAs (Figure 2). The full field of view (FOV) measures 15x15x15cm spherically while the ‘upper jaw’ and ‘lower jaw’ settings collimate to a display volume with an approximate height of 8.5cm and therefore about 8.5 x 15 x 15 cm.⁴⁵







					
85 kV/ 10 mAs	85 kV/ 14 mAs	85 kV/ 21 mAs	85 kV/ 28 mAs	85 kV/ 35 mAs	85 kV/ 42 mAs

Figure 2: Available Exposure Settings for GALILEOS® Comfort

Current is 7mA except for 10mAs for which current is 5mA

A review of the current literature was conducted in order to identify studies investigating dosimetry associated with the Sirona Galileos® CBCT scanner. A search was completed using search terms ‘cone beam computed tomography’, ‘dosimetry’ and associated abbreviations and truncated terms. Literature databases included PubMed, BIOSIS, EMBASE, CINAHL and Dissertations and Theses. Studies matching initial search criteria were combined and reviewed by title and abstract. Papers relevant to the research question were reviewed to determine the inclusion of the Sirona GALILEOS® Comfort CBCT scanner. As of the writing of this thesis, only 3 such papers were identified.

Ludlow and Ivanovic⁴⁶ investigated the dosimetry associated with 8 dentoalveolar and maxillofacial CBCT units, including the Sirona GALILEOS®, as well as a 64-slice MDCT unit. Absorbed dose was measured for 24 select sites in the head and neck region using thermoluminescent dosimeter (TLD) chips and a radiation analog dosimetry (RANDO®) phantom. Effective dose was calculated to be 70 μ Sv for default exposure (full FOV, 21mAs) and 128 μ Sv for maximum exposure (full FOV, 42mAs) based on 2007 ICRP¹ tissue weighting factors.

Pauwels et al⁴⁷ determined the effective dose for a wide range of CBCT scanners and protocols including the GALILEOS® Comfort.⁴⁷ Absorbed dose was measured using between 147 – 152 TLD chips in anthropomorphic (ART) phantoms. The effective dose for the Sirona GALILEOS® Comfort using a full FOV (15x15x15cm), 85kV and 28mAs was measured to be 84 μ Sv. Effective dose was also calculated based on 2007 ICRP¹ tissue weighting factors. The authors claim an improved accuracy as a result of an increased number and distribution of TL dosimeters throughout the phantom.

Rottke et al⁴⁸ evaluated the span of effective doses associated with ten different CBCT scanners including the GALILEOS® Comfort. Absorbed dose was measured using TL dosimeters placed in 24 sites in a RANDO® phantom following the protocol of Ludlow.⁴⁶ The effective dose span was established by measuring the doses for the lowest and highest exposure protocols. The minimum exposure protocol using a full FOV, voxel size 0.15mm³ and current 7mA resulted in an effective dose of 51 μ Sv. Since the 10mAs exposure setting uses a reduced current of 5mA, it is assumed the authors set the exposure at 14mAs. The maximum exposure protocol using a full

FOV, 0.3mm³ voxel size and 7mA (42mAs) current (/exposure) resulted in a measured effective dose of 95µSv. Effective dose was again calculated based on 2007 ICRP¹ tissue weighting factors.

PURPOSE

While the number of dosimetry studies relating to CBCT units used in dentistry continues to increase, few have reported findings associated with the Sirona GALILEOS® Comfort scanner for its full range of operation. A review of the literature identified three such studies in which only a restricted number of protocols were investigated. All protocols described were of full maxillomandibular scans. With regard to exposure time, pooled data reveals effective dose associated with mAs settings of 14, 21, 28 and 42. However, no single published study was identified comparing the effective dose for a range of exposure and FOV settings.

The purpose of this thesis is to determine and compare the dosimetry associated with different scanning protocols available with the Sirona GALILEOS® Comfort CBCT scanner. This information should assist in determining the optimal scanning protocol for each patient when combined with knowledge of respective effects on image quality.

MATERIALS AND METHODS

Absorbed dose was measured using optically stimulated luminescent (OSL) dosimeters placed within a single, modified, male tissue-equivalent Alderson RANDO® phantom.

Dosimeters

Absorbed dose was measured at established sites using InLight® nanoDot™ OSL dosimeters (Landauer, Glenwood, Ill). OSL dosimeters offer a wide operating energy range, efficient readings and reanalysis capabilities with minimal angular and energy dependence.³⁸

In total, 27 OSL dosimeters were used throughout the study. All dosimeters were calibrated using a Therapax HF150 superficial radiation therapy x-ray unit (Pantak, East Haven, CT) with a 1.1mm Al +0.3mm Cu filter. This filter allowed for production of a beam quality similar to that of the GALILEOS® Comfort confirmed by measurement of the respective Half Value Layer (HVL). The Therapax unit allows user control over kVp, mA, exposure time and source to object distance. Groups of OSL dosimeters not exceeding the beam field were positioned flat on a Polymethyl methacrylate (PMMA) block 140mm in height (Figure 3). This platform approximated the dimensions of the human phantom to account for similar amounts of backscatter radiation. The OSL dosimeters were exposed at fixed dose intervals and read until the cumulative count exceeded the maximum count of the OSL dosimeters used for phantom protocols. Each OSLD was read using a microstar OSLD reader (Landauer, Glenwood, Ill), taken as the average of three repeated readings. Each exposure was measured under identical conditions using a Farmer Chamber and Capintec 192 Digital Exposure Meter (Capintec, Ramsay NJ) with calibration traceable to national standards. Respective calibration curves were established to characterize each individual OSLD and obtain corrected dose from each OSLD reading. Appropriate adjustments were made for room temperature and pressure.



Figure 3: Therapax HF 150

1.1mm Al + 0.3mm Cu filter, Farmer Chamber & PMMA background

Phantom

The head and neck segment of the RANDO® phantom consists of 10 sections, each with predrilled holes designed to accommodate thermoluminescent dosimeters (TLDs). In order to place OSL dosimeters, five PMMA templates (Figure 4) 2.15mm thick were fabricated and placed superior to sections three, four, six, seven and nine (Figure 5). In diagnostic radiology, PMMA is the most tissue equivalent material used.⁴⁹ Square holes were placed in each template large enough to accommodate OSL dosimeters at anatomical landmarks without allowing movement.



Figure 4: PMMA template for OSLD placement



Figure 5: RANDO® phantom with PMMA templates in place

Anatomic Landmarks

Twenty six sites were measured corresponding to the 24 anatomical positions described by Ludlow (Table 5).⁵⁰ Two sites each were established for the left and right mandibular body. Due to difficulty approximating the centre of the body, one site was positioned superior to and another inferior to the mandibular body with the average absorbed dose representing that of the mandibular body. An additional OSLD was used to measure background radiation and was present beside the operator during acquisition and remained with the other dosimeters during transport.

<i>Anatomic Location</i>	<i>OSLD Number</i>	<i>OSLD ID</i>
Calvarium anterior	1	34151D
Calvarium left	2	42477T
Calvarium posterior	3	42098X
Midbrain	4	44986I
Pituitary	5	46848I
Right orbit	6	29436W
Left orbit	7	48908I
Right lens of eye	8	41606Z
Left Lens of eye	9	46757L
Right cheek	10	409410
Right parotid	11	27592Y
Left parotid	12	37841X
Right ramus	13	26177Z
Left ramus	14	32758P
Centre cervical spine	15	31835W
Left back of neck	16	44131D
Right mandible body upper	17	45032C
Right mandible body lower	18	35299O
Left mandible body upper	19	32817T
Left mandible body lower	20	48629K
Right submandibular gland	21	31657U
Left submandibular gland	22	32871Z
Centre sublingual gland	23	28791V
Midline thyroid	24	46970B
Thyroid surface - left	25	294126
Esophagus	26	35015A
Background	27	321268

Table 5: Anatomic sites for dosimeter placement

Each phantom is constructed of a natural human skeleton cast inside a standard mold composed of a material radiologically simulating soft tissue. Initial images of the phantom revealed discrepancies between soft tissue contours of the head and neck and the underlying skeleton (Figure 6). Dosimeter sites for skeletal and internal soft tissue landmarks were established in relation to the skeleton while surface landmarks were established with respect to soft tissue sites on the RANDO® phantom. Surface landmarks were marked with tape over which OSL dosimeters were centred for each protocol.

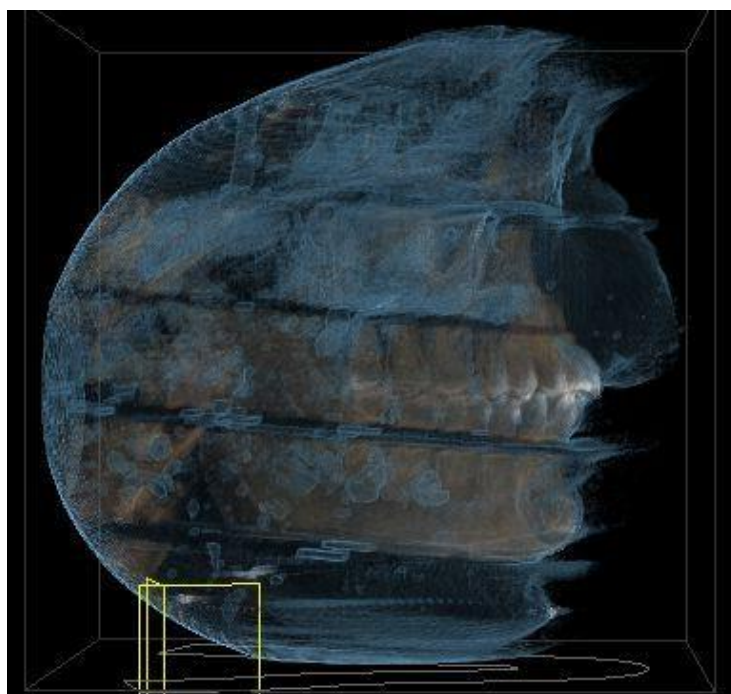


Figure 6: Relationship of hard and soft tissue in RANDO® phantom

With the PMMA templates in place, lead foil from intraoral radiograph packets was placed in each internal OSLD location and a 3D scan completed. The reconstructed image was examined to confirm acceptable location of each internal landmark (Figure 7).

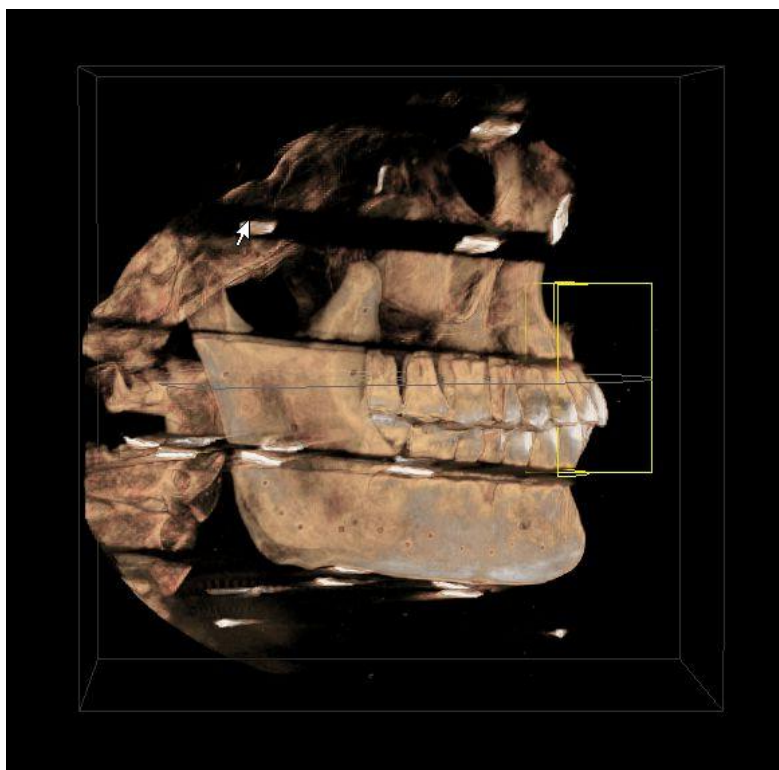


Figure 7: Lateral Cephalometric view with lead foil at OSLD locations

Phantom Orientation

The RANDO® phantom was oriented with the occlusal plane parallel to the scan plane, the outline of the soft tissue chin and nose visible and both inferior and posterior borders of the mandible superimposed. After an acceptable setup was obtained, the Volume Control Head mount supplied for the Sirona GALILEOS® was modified with three wires extending from custom acrylic attachments (Figure 8). The tips of each wire corresponded to surface points on the phantom marked with tape. This allowed for reproduction of the setup between protocols. The image from each protocol was examined and deemed acceptable if the ‘rotation’ and ‘tilt’ settings required to establish optimal superimposition of the right and left borders of the mandible did not exceed ± 1 unit of rotation or tilt correction (Figure 9).



Figure 8: Modified mount for setup reproduction

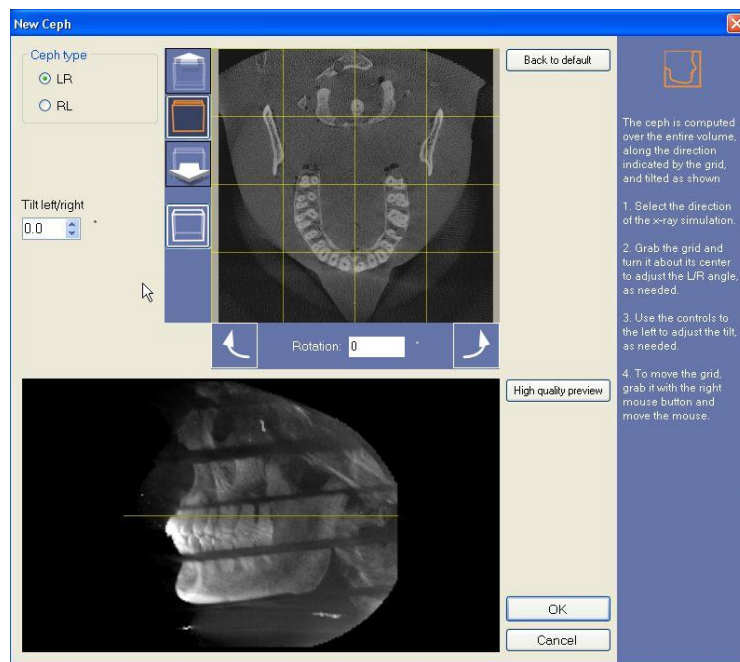


Figure 9: 'Tilt' and 'Rotation', confirming setup reproduced

Protocols

With three fields of view, six mAs and two contrast and resolution settings available, a total of 72 protocols are possible with the Sirona Galileos® Comfort CBCT scanner. Of these 72 protocols a total of 12 were investigated, chosen as a representative sample of those available. In choosing these 12 protocols, those most commonly used are included and sufficient protocols were selected to allow changes in one parameter while keeping the remaining 3 unchanged. The protocols selected are summarized in Table 6. Protocol #1 (Full FOV 42mAs VO1HC) was repeated on three separate occasions to investigate variability in effective dose calculations between repeated protocols.

<i>Protocol #</i>	<i>Field of View</i>	<i>mAs</i>	<i>Resolution</i>	<i>Contrast</i>
1	Mandibular	14	VO1	High
2	Mandibular	28	VO1	High
3	Mandibular	42	VO1	High
4	Maxillary	14	VO1	High
5	Maxillary	28	VO1	High
6	Maxillary	42	VO1	High
7	Full	14	VO1	High
8	Full	28	VO1	High
9	Full	42	VO1	High
10	Full	42	VO1	Normal
11	Full	42	VO2	High
12	Full	42	VO2	Normal

VO1 = High Resolution Setting
VO2 = Standard Resolution Setting

Table 6: Summary of protocols investigated

Prior to each protocol, room temperature and pressure were measured using a Traceable Digital Workstation Barometer (VWR International, Mississauga Ont.). A certificate is provided from

an ISO 17025 calibration laboratory accredited by A2LA to indicate instrument traceability to standards provided by the National Institute of Standards and Technology.

Each scanning protocol was repeated three times prior to removing the OSL dosimeters from the phantom to minimize the contribution of noise to absorbed dose. Absorbed dose was thus obtained by dividing the dose measured by three. At least 15 minutes was ensured between scanning and reading the dosimeters as suggested by the manufacturer. This allows low-level, non-dosimetric electron traps to stabilize.³⁸

The dosimeters were read using a microstar OSLD reader (Landauer, Glenwood, Ill) taking the mean value of three subsequent readings. They were annealed using a high intensity light source (Figure 10) after no more than three subsequent protocols to minimize the increase in measurement uncertainty associated with dose accumulation.

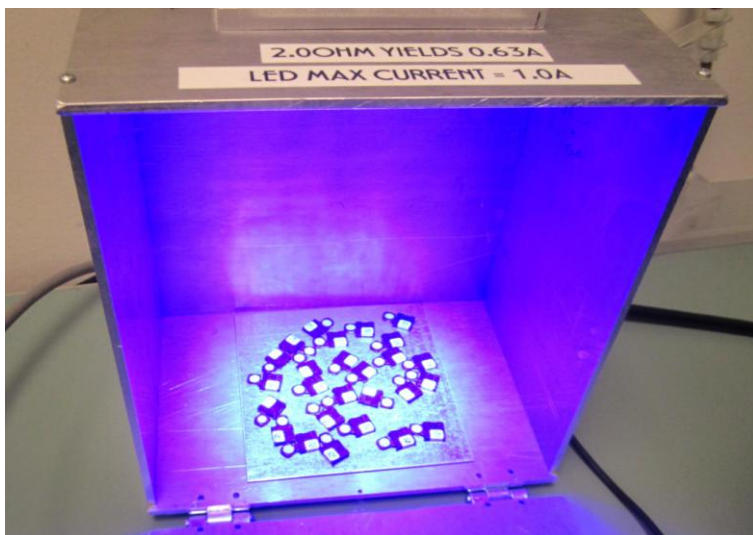


Figure 10: High intensity light source to anneal OSL dosimeters

Dosimeter counts were entered into a spreadsheet and absorbed dose determined by means of applying individual calibration curves. Effective dose was calculated using the mean absorbed dose to the individual tissues and organs, applying the corresponding 2007 ICRP¹ tissue weighting factors and correcting for the fractional volume of tissue irradiated. The fraction of tissue irradiated was determined by following that outlined by Ludlow and Ivanovic.⁴⁶ A correction factor of 2.76 was applied for bone surface dose relative to bone marrow dose based

on the ratio of mass energy absorption coefficients for bone and muscle. The ratio is energy dependent and was chosen for a kVp of 85 and Half Value Layer (HVL) of 7mm of Aluminum.⁵¹ However a correction for enhanced backscatter from bone was not applied.⁵² Table 7 lists the dosimeters used to sample each tissue and summarizes the respective fraction of tissue irradiated and tissue weighting factors. For those tissues located outside of the head and neck, absorbed dose was assumed to be negligible.

<i>Tissue/Organ</i>	<i>ID of OSLDs Used to Sample Tissue</i>	<i>Fraction of Tissue Irradiated (%)</i>	<i>Tissue Weighting Factor (W_T)</i>
Red bone marrow		16.5	0.12
Mandible	13, 14, 17-20	1.3	
Calvaria	1, 2, 3	11.8	
Cervical Spine	15	3.4	
Oesophagus	26	10	0.04
Thyroid	24, 25	100	0.04
Skin	8, 9, 10, 16	5	0.01
Bone surface		16.5	0.01
Mandible	13, 14, 17-20	1.3	
Calvaria	1, 2, 3	11.8	
Cervical Spine	15	3.4	
Brain	4,5	100	0.01
Salivary Glands	11, 17-23, 12, 21, 22, 23	100	0.01
Remainder			0.12
Lymphatic nodes	11-15, 17-24, 26	6	
Muscle	11-15, 17-24, 26	6	
Extrathoracic Airway	6, 7, 11-15, 17-24, 26	100	
Oral mucosa	11-14, 17-23	100	
Gonads		0	0.08
Colon		0	0.12
Lung		0	0.12
Stomach		0	0.12
Bladder		0	0.04
Breast		0	0.12
Liver		0	0.04

Table 7: Percentage tissue irradiated, tissue weighting factor and OSLD sample for each tissue/organ

RESULTS

A summary of the effective dose associated with each protocol is presented in Table 8, each based on 2007 ICRP¹ tissue weighting factors (Table 3). The effective dose span ranged from 36 μSv for a maxillary scan at 14mAs to 142 μSv for a full maxillomandibular scan at 42mAs. This is equivalent to between 5 and 22 days of per capita background radiation based on a world annual average of 2400 μSv .³⁰

<i>Protocol</i>	<i>Field of View</i>	<i>mAs</i>	<i>Contrast</i>	<i>Resolution</i>	<i>Effective Dose (μSv) (ICRP 2007)¹</i>	<i>Days per capita background (2007)*</i>
1	Mandibular	14	High	High	37	6
2	Mandibular	28	High	High	74	11
3	Mandibular	42	High	High	107	6
4	Maxillary	14	High	High	36	5
5	Maxillary	28	High	High	69	11
6	Maxillary	42	High	High	100	15
7	Full	14	High	High	48	7
8	Full	28	High	High	95	14
9	Full	42	High	High	142	22
9	Full	42	High	High	140	21
9	Full	42	High	High	141	22
10	Full	42	High	Standard	142	22
11	Full	42	Normal	High	142	22
12	Full	42	Normal	Standard	140	21

Table 8: Effective dose calculations for protocols completed

*assuming world average of 2400 $\mu\text{Sv}/\text{year}$ ³⁰

The full maxillomandibular scan at 42mAs, high contrast and high resolution was repeated on three separate occasions (Protocol #9). The effective dose calculated for each was 140, 141 and 142 μSv . Minimal variability in effective dose was associated with dosimeter placement and phantom orientation between protocols.

Collimating for a maxillary or mandibular scan resulted in a reduced effective dose relative to a full maxillomandibular scan. Table 9 shows the effective dose for both maxillary and mandibular scans as a percentage of a full scan for each mAs investigated. All scans were high resolution and high contrast. The effective dose associated with a full maxillomandibular scan is reduced on average by 28% when collimated for a maxillary scan and 23% when collimated for a mandibular scan. This exceeds the 15% approximation reported by Sirona.⁴⁵

<i>Field of View</i>	<i>14mAs</i>	<i>28mAs</i>	<i>42mAs</i>	<i>Mean</i>
Maxillary	74%	73%	70%	72%
Mandibular	78%	78%	76%	77%

Table 9: Effective dose of collimated scans as a percentage of full maxillomandibular scan dose by mAs

Figure 11 depicts the changes in effective dose with increasing mAs for maxillary, mandibular and full fields of view. All scans were at high resolution and contrast. Both maxillary and mandibular scans show a similar effective dose reduction relative to a full scan throughout the range of mAs settings. This difference increases in magnitude with increasing mAs. An increase in mAs results in a linear and proportional increase in effective dose for all fields of view.

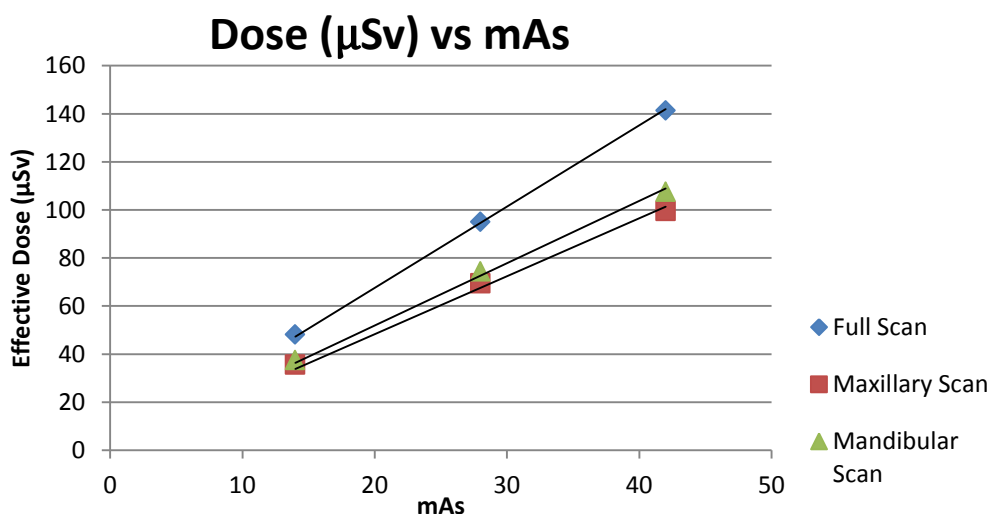


Figure 11: Effective Dose vs mAs

The mean equivalent dose to individual organs and tissues is summarized in Table 10. Table 11 compares the equivalent doses for maxillary scans as a percentage of the equivalent doses for mandibular scans, taking the mean of 14, 28 and 42 mAs percentages. While the effective doses for maxillary and mandibular scans are similar, the distribution of equivalent doses to the tissues differs. For a maxillary scan, the equivalent dose to the brain is on average 298% of that for a mandibular scan and similarly 146% for skin and 140% for bone marrow.

Protocol	Bone Marrow	Thyroid	Esophagus	Skin	Bone Surface	Salivary Glands	Brain	Remainder Tissues			
								Lymphatic Nodes	Extrathoracic Region	Muscle	Oral Mucosa
Full 14mAs VO1HC	73	112	4	36	202	1104	447	889	856	889	1020
Full 28mAs VO1HC	139	233	19	67	382	2225	776	1793	1719	1793	2042
Full 42mAs VO1HC #1	208	335	32	98	573	3372	1150	2683	2582	2683	3058
Full 42mAs VO1HC #2	206	351	30	100	568	3296	1108	2638	2536	2638	3005
Full 42mAs VO1HC #3	211	327	33	102	583	3328	1144	2665	2557	2665	3025
Full 42mAs VO1NC	201	359	31	102	555	3418	1109	2659	2559	2659	3028
Full 42mAs VO2HC	211	322	30	105	582	3363	1157	2686	2584	2686	3065
Full 42mAs VO2 NC	206	326	29	105	567	3320	1123	2646	2546	2646	3021
Max 14mAs VO1HC	69	45	0	29	189	707	442	632	630	632	710
Max 28mAs VO1HC	131	97	5	62	361	1399	785	1242	1239	1242	1383
Max 42mAs VO1HC	185	145	10	93	511	2016	1090	1793	1794	1793	1989
Mand 14mAs VO1HC	51	90	3	25	139	956	196	782	701	782	909
Mand 28mAs VO1HC	94	204	13	41	260	1966	257	1588	1413	1588	1830
Mand 42mAs VO1HC	129	299	24	56	355	2917	301	2327	2068	2327	2687

VO1 = High Resolution
VO2 = Standard Resolution
HC = High Contrast
NC = Normal Contrast

Table 10: Equivalent dose (μSv) to tissues/organs

Bone Marrow	Thyroid	Esophagus	Skin	Bone Surface	Salivary Glands	Brain	Lymphatic Nodes	Extrathoracic Region	Muscle	Oral Mucosa
140%	49%	27%	146%	140%	71%	298%	79%	88%	79%	76%

Table 11: Equivalent doses for maxillary scan as a percentage of equivalent doses for mandibular scan (taken as mean of percentages for 14, 28 and 42 mAs)

Table 12 summarizes the effective dose for protocols where contrast and resolution were changed while field of view and mAs were kept at full maxillomandibular and 42 respectively. Effective dose was within 2 μSv for these protocols suggesting that changes in contrast and/or resolution have little if any impact on effective dose.

<i>Protocol</i>	<i>Field of View</i>	<i>mAs</i>	<i>Contrast</i>	<i>Resolution</i>	<i>Effective Dose (μSv) (ICRP 2007)¹</i>	<i>Days per capita background (2007)*</i>
9	Full	42	High	High	141	22
10	Full	42	High	Standard	142	22
11	Full	42	Normal	High	142	22
12	Full	42	Normal	Standard	140	21

Table 12: Effect of resolution and contrast on dose

DISCUSSION

The mean effective dose calculated for the maximum exposure (maxillomandibular scan, 42mAs, high contrast, high resolution) was 141 μSv . This compares with previous findings, Ludlow and Ivanovic⁴⁶ who reported 128 μSv and Rottke et al⁴⁸ who reported 95 μSv . The effective dose calculated for a maxillomandibular scan at 28mAs (high contrast, high resolution) was 95 μSv compared to 84 μSv reported by Pauwels et al.⁴⁷ All reports are based on 2007 ICRP¹ tissue weighting factors. It is important when making comparisons between studies that the same weighting factors are used. In general, effective dose based on 1990 ICRP tissue weighting factors is significantly reduced relative to 2007 due to the increased weighting factors for salivary gland tissue and brain introduced in 2007.

During this study, calibration curves for each OSLD were initially established by two methods. The method used in this study simulated conditions of surface dosimeters ('free in air' with PMMA background) while the other simulated conditions of dosimeters placed internally by placing them under 5cm of PMMA. A 5cm PMMA barrier was chosen when it was estimated that the beam was attenuated by an average of 5cm of phantom tissue prior to reaching the internal dosimeters. The 'free in air' method with a PMMA background was chosen for the definitive calibration method in order to minimize the risk of underestimating effective dose. Preliminary calculations using 'in plastic' calibration curves determined an effective dose of 102 μSv for a full scan at 42 mAs as compared to the definitive calculation of 141 μSv using 'in air' calibration.

The discrepancy between effective dose calculations based on 'free in air' and 'in plastic (PMMA)' calibration curves reveals the importance of the calibration process in obtaining accurate effective dose estimates. Ludlow and Ivanovic⁴⁶ reported the use of thermoluminescent dosimeters that were precalibrated and analyzed by the supplier Lindauer (Glenwood, IL). It is unclear under what conditions respective calibration curves were established. Pauwels et al⁴⁷ reported the use of two types of TLDs, one type calibrated free in air, the other by calibrating internal calibration dosimeters for each experiment. Rottke et al⁴⁸ calibrated each TLD to obtain individual calibration factors. Those with calibration factors outside two standard deviations were excluded while an average calibration factor was used for

effective dose calculation. There is no mention whether calibration was completed ‘free in air’ or under different conditions.

An additional property that is significant when using dosimeters is their angular dependence. It is possible that the orientation of a dosimeter to the primary beam affects the dose measured. Thermoluminescent dosimeters are directionally independent.³⁵ There is conflicting evidence with regard to the angular dependence of OSL dosimeters with a study by Jursinic³⁸ finding no angular dependence when exposed to 50 cGy of 6 MV x-rays while Kerns et al⁴² report a 3-4% variation in OSLD response with variation in dosimeter orientation relative to a 6 and 18MV photon beam. It may be ideal to calibrate the dosimeters at their defined positions in the RANDO® phantom to circumvent the issues of orientation and ‘in air’ versus ‘in plastic’ calibration. However, there is no means to acquire standardized reference dose measurements at these sites using an ion chamber.

This study aimed to identify the effect of each parameter on effective dose. A reproducible set-up is of great importance such that comparisons can be made between different protocols. Once an acceptable position of the phantom was obtained, a modified Volume Control Head Mount was used to reproduce positioning based on three surface points. After each protocol the ‘tilt’ and ‘rotation’ settings were modified to obtain optimal superimposition of the posterior and inferior borders of the mandible. A set-up was deemed to be adequately reproduced if these settings did not deviate more than ± 1 tilt or rotation correction unit. This range was established arbitrarily prior to the study. It is unclear if the tilt and rotations settings correspond to a given number of degrees but it was observed that modifying the tilt or rotation ± 1 corresponded to relatively little movement of the image. Using the modified head mount proved successful with every protocol adequately reproducing the original. To investigate the reproducibility of effective dose measurement, a maxillomandibular protocol with maximum exposure (42mAs, high contrast, high resolution) was repeated on three separate occasions. The effective dose was very similar measuring 140, 141 and 142 μSv .

Thermoluminescent dosimeters have been used with success for many decades and account for the majority of dosimeters used in organ dose phantom studies in dentistry. As a result, most phantoms in use are prepared with predrilled holes to accommodate TL dosimeters. These are

often cylindrical and smaller in size than the InLight® nanoDot™ OSL dosimeter (Landauer, Glenwood, Ill) used in this study. Optically stimulated luminescent dosimeters were chosen for use in this study as they were already in established use in our associated clinical cancer therapy facility. They offer acceptable accuracy and precision, less dependence on technique and operator and less concerns with respect to signal fading between radiation exposure and readout. A review of the literature revealed only one dental CBCT dosimetry study using OSL dosimeters. Al Najjar et al⁵³ compared the adult and child radiation equivalent dose from two dental CBCT units. They used OSL dosimeters of unspecified type and head phantoms manufactured specifically to accommodate OSL dosimeters. Comparing results between studies can be difficult due to differences in phantom and dosimeters used. In this study, a RANDO® phantom previously prepared for use with TL dosimeters was modified to accommodate OSL dosimeters using five 2.15mm thick PMMA templates designed to fit between the phantom sections. This effectively increases the dimensions of the phantom by approximately 11mm and could therefore affect absorbed doses by displacing OSL dosimeters located more superiorly and inferiorly further from the primary beam. While PMMA is commonly used in dosimetry studies due to its tissue equivalent properties, its attenuation value may differ from that of the RANDO® phantom.

An advantage of TL dosimeters for the phantom used is the potential to place the dosimeters anywhere within the phantom. With the modified phantom, OSL dosimeter placement was restricted to the PMMA templates between phantom sections. Initial images revealed that the skull was not well related to the soft tissue contours with the hard tissue chin displaced quite superiorly. Each phantom is composed of a natural human skull cast inside a standard soft tissue mold and thus each phantom is unique. Variations in the natural skulls between phantoms could affect the appropriate section for dosimeter placement and the relationship of tissues and structures to the primary beam. In this study we chose to place internal dosimeters according to hard tissue references and external dosimeters according to soft tissue landmarks. Accuracy in the spatial relationship between internal and external dosimeters was limited by the phantom anatomy. The phantom was oriented with the goal of maximizing hard tissue structures and soft tissue contours of interest. It is possible that superior and inferior structures were further displaced from the primary beam due to the anatomy of the phantom. An image obtained with lead foil in place of dosimeters revealed reasonable approximation to the tissues and structures of

interest. While the phantom anatomy and need for modification to accommodate OSL dosimeters does present some limitations, comparisons between protocols within the study remain valid.

Optically stimulated luminescent dosimeters were selected for this study. They provide a more efficient and less technique sensitive reading than TL dosimeters and not subject to the same degree of fading. They have good accuracy and precision and are suitable for dosimetry studies. A logistical advantage of OSL dosimeters is the potential for incremental use where, unlike TLDS, minimal charge is lost during analysis (0.04-0.25%).⁵⁴ The manufacturer discourages continued incremental use since a supralinear dose response is noted when accumulated dose exceeds 300cGy and the uncertainty of measurements can increase from 2% to as much as 4%. A 100 cGy dose corresponds to an approximate signal of 130 000 counts with the OSL dosimeter used.³⁸ For logistical reasons, OSL dosimeters were used for incremental measures with up to three protocols measured prior to annealing for re-use. The accumulated signal did not exceed 100 000 counts and therefore well within the range of a linear dose response.

One comparison of interest is the effect of resolution and contrast settings on effective dose. With the Sirona GALILEOS® Comfort CBCT scanner, the user has the options of high or standard contrast and resolution settings. A full maxillomandibular scan was completed at 42mAs for all 4 resolution and contrast combinations. There was no significant difference in effective dose between the four protocols. The manufacturer reports that both high and standard resolution options produce a data volume set with 512 x 512 x 512 voxels. The high-resolution secondary reconstruction can be generated by the software only if the high-resolution setting is selected. Specific information regarding the difference between high and standard settings for resolution and contrast proved difficult to obtain. Limited information available suggested that pixel binning occurs if the high-resolution setting is selected thus transferring data with a voxel size of 0.3mm but maintaining the capability of reconstructing an image with 0.15mm voxel size post acquisition. The standard resolution does not maintain this capability but may as a result allow for faster data transfer. These results suggest that there is little benefit in selecting the standard resolution setting and contrast settings should be chosen based on optimizing the tissues of interest. It is likely the same projection set is acquired regardless of the contrast and resolution software settings selected prior to image acquisition.

An important clinical decision when obtaining a CBCT image is selecting the field of view as additional information can be obtained with a larger field of view but at the expense of increased patient exposure. This decision will be based on potential structures of clinical interest and the associated dose incurred when acquiring the image. The results of this study suggest that collimating to a maxillary or mandibular scan results in a reduction in effective dose of approximately 28% and 23% respectively, this exceeds the approximate 15% reported by the manufacturer. It should be noted that no modifications were made to the percentage of tissue irradiated when calculating the effective dose for partial scans. It could be argued that respective reductions should be made which could result in additional reduction in effective dose when partial scans are selected. A review of previous literature revealed only one study adjusting fraction of tissue irradiated for partial scans with adjustments based on the opinion of the local radiologist.⁵⁵ No modification to the fraction of tissue irradiated was elected as it was observed that all dosimeters registered a significant dose for partial scans. This ‘conservative’ approach reduces the risk of under reporting the effective dose but may as a result neglect to report the full benefit in dose reduction when selecting a collimated protocol. Based on these findings it is apparent a moderate reduction in effective dose is realized when selecting a partial scan. However, if structures present on a full scan are omitted by collimation and may be of interest in the future, consideration towards a full scan is justified as the cumulative dose of two separate partial scans is likely to exceed that of a full scan.

The primary aim of this study was to investigate the impact different parameters had on effective dose. Ideally each of the 72 potential protocols would be investigated individually. This would allow more robust statistical analysis of linearity when comparing effective dose with changes in mAs. In addition, changes in contrast and resolution settings were investigated only for full maxillomandibular scans at 42mAs. While a similar data acquisition process is likely for the remaining field of views and mAs settings, this cannot not be concluded with certainty.

Effective dose is important when determining the optimum scanning protocol for an individual patient and clinical question. The information provided by this study is useful in understanding the relative effects each parameter has on effective dose. It is important to understand that establishing an optimum protocol must also consider image quality. Collimation reduces the amount of structures visible on the image while changes in mAs, contrast and resolution can and

often do impact the image quality. Such changes may or may not impact diagnosis. Future study of the impact of the same parameters on image quality (e.g. standard tests of spatial and contrast resolution) would provide equally important information in determining optimum scanning protocols using the Sirona Galileos® CBCT scanner.

SUMMARY

The aim of this study was to measure and compare the effective dose associated with a sample of protocols available using the Sirona GALILEOS® Comfort CBCT scanner. With this unit the tube voltage and number of basis projections are set by the manufacturer to 85kVp and 200 respectively. The user can establish a protocol by selecting between mAs, contrast, resolution and collimation settings. This study investigated 12 protocols with modifications to all four parameters.

Results revealed a dose span of 48 μ Sv to 142 μ Sv for a full maxillomandibular scan, relatively low when compared to conventional CT units but significantly higher than panoramic and lateral cephalometric exposures. Effective dose varied linearly with mAs while contrast and resolutions settings had little impact on effective dose for this scanner. A moderate reduction in effective dose can be realized when collimating for a partial scan.

Cone beam computed tomography can provide significant diagnostic value when prescribed appropriately. Further evidence is needed to clarify when the clinical benefit justifies the burden of additional radiation exposure. When a CBCT image is justified, the results of this study will assist the clinician in determining the optimum protocol for each patient when considered in the context of diagnostic or treatment planning applications.

CONCLUSIONS

This study demonstrates the importance of setting individualized patient exposure protocols in order to minimize patient dose from ionizing radiation used for diagnostic or treatment planning tasks. This observation is supported by the following conclusions:

The highest mean effective dose calculated was for a full maxillomandibular scan at maximum (42) mAs was 141 μ Sv based on 2007 ICRP¹ tissue weighting factors. The lowest mean effective dose was 36 μ Sv for a maxillary scan at 14mAs.

1. Collimating to obtain a maxillary or mandibular scan decreased effective dose by approximately 28% and 23% respectively.
2. Changes to mAs and beam collimation have a significant influence on effective dose.
3. Changes in contrast and resolution software settings have little impact on effective dose with the Sirona GALILEOS® CBCT scanner.
4. Effective dose varies linearly with mAs.

This work has established a comprehensive baseline of dosimetric findings for subsequent comparison of image quality indicators in phantoms and clinical images obtained by each Galileos Comfort protocol. The goal remains to optimize radiation exposure to “as low as is reasonably achievable”, while achieving the intended clinical benefit to the patient.

REFERENCES

1. ICRP. The 2007 recommendations of the international commission on radiological protection. ICRP publication 103. *Ann ICRP*. 2007;37:2-4.
2. White SC, Pharoah MJ. *Oral radiology :Principles and interpretation*. 6th ed. St. Louis, Mo.: Mosby/Elsevier; 2009:641.
3. Scarfe WC, Farman AG, Sukovic P. Clinical applications of cone-beam computed tomography in dental practice. *J Can Dent Assoc*. 2006;72(1):75-80.
4. ICRP. The optimisation of radiological protection: Broadening the process. ICRP publication 101. approved by the commission in september 2005. *Ann ICRP*. 2006;36(3):65, 71-104.
5. National Council on Radiation Protection and Measurements. *Radiation protection in dentistry :Recommendations of the national council on radiation protection and measurements (report no. 145)*. Vol 145. Bethesda, MD: National Council on Radiation Protection and Measurements; 2003:191.
6. American Dental Association Council on Scientific Affairs. The use of cone-beam computed tomography in dentistry: An advisory statement from the american dental association council on scientific affairs. *J Am Dent Assoc*. 2012;143(8):899-902.
7. Iannucci JM, Iannucci JM. *Dental radiography :Principles and techniques*. 4th; 4th ed. St. Louis, Mo.; St. Louis, Mo.: Elsevier/Saunders; Elsevier/Saunders:466; 466.
8. Kantor ML. Dental digital radiography: More than a fad, less than a revolution. *J Am Dent Assoc*. 2005;136(10):1358, 1360, 1362.

9. Mouyen F, Benz C, Sonnabend E, Lodter JP. Presentation and physical evaluation of RadioVisioGraphy. *Oral Surgery, Oral Medicine, Oral Pathology*. 1989;68(2):238-242.
10. Crawford PR. 100 years of radiology: Those early years. *J Can Dent Assoc*. 1995;61(11):951-954.
11. Finlay LM. Craniometry and cephalometry: A history prior to the advent of radiography. *Angle Orthod*. 1980;50(4):312-321. doi: 2.
12. Pacini AJ. Roentgen ray anthropometry of the skull. *J Radiol*. 1922(3):230-238, 322-331, 418-426.
13. Allen WI. Historical aspects of roentgenographic cephalometry. *Am J Orthod*. 1963;49(6):451-459.
14. Seynaeve PC, Broos JI. The history of tomography. *J Belge Radiol*. 1995;78(5):284-288.
15. Hallikainen D. History of panoramic radiography. *Acta Radiol*. 1996;37(3 Pt 2):441-445.
16. Frank ZA. Panoramic x-ray apparatus. . 1922(1408559).
<http://www.freepatentsonline.com/1408559.html>.
17. PAATERO YV. Radiography of the temporo-mandibular joint; a new method. *Ann Chir Gynaecol Fenn*. 1953;42(4):259-264.
18. PAATERO YV. Geometrical study on possibilities of making double eccentric pantomograms with a single exposure. *Suom Hammaslaak Toim*. 1954;50(Suppl. 2):36-43.
19. PAATERO YV. Pantomography in theory and use. *Acta Radiol*. 1954;41(4):321-335.

20. PAATERO YV. Pantomography of spherical layers. *Acta Radiol.* 1957;48(3):181-187.
21. Dove SB, McDavid WD, Welander U, Tronje G. Preliminary evaluation of a digital system for rotational panoramic radiography. *Oral Surg Oral Med Oral Pathol.* 1992;73(5):623-632.
22. McDavid WD, Dove SB, Welander U, Tronje G. Electronic system for digital acquisition of rotational panoramic radiographs. *Oral Surg Oral Med Oral Pathol.* 1991;71(4):499-502.
23. Kashima I, Kanno M, Higashi T, Takano M. Computed panoramic tomography with scanning laser-stimulated luminescence. *Oral Surg Oral Med Oral Pathol.* 1985;60(4):448-453.
24. Kalender W. *Computed tomography :Fundamentals, system technology, image quality, applications.* 3 rev ed. Erlangen: Publicis Corporate Pub.; 2011:372.
25. Hsieh J, Society of Photo-optical Instrumentation Engineers. *Computed tomography.* 2nd ed. Bellingham, Wash. 1000 20th St. Bellingham WA 98225-6705 USA: Spie; 2009:556.
26. Hatcher DC. Operational principles for cone-beam computed tomography. *J Am Dent Assoc.* 2010;141 Suppl 3:3S-6S.
27. Nemtoi A, Czink C, Habu D, Gahleitner A. Cone beam CT: A current overview of devices. *Dentomaxillofac Radiol.* 2013;42(8):20120443.
28. Miracle AC, Mukherji SK. Conebeam CT of the head and neck, part 2: Clinical applications. *AJNR Am J Neuroradiol.* 2009;30(7):1285-1292.
29. van Vlijmen OJ, Kuijpers MA, Berge SJ, et al. Evidence supporting the use of cone-beam computed tomography in orthodontics. *J Am Dent Assoc.* 2012;143(3):241-252.

30. United Nations Scientific Committee on the Effects of Atomic Radiation. "Annex B: Exposures from natural radiation sources", UNSCEAR 2000 report. . 2000.
31. Stabin MG. *Radiation protection and dosimetry :An introduction to health physics*. New York, NY: Springer; 2008:378.
32. Thilander-Klang A, Helmrot E. Methods of determining the effective dose in dental radiology. *Radiat Prot Dosimetry*. 2010;139(1-3):306-309.
33. Boone JM. The trouble with CTD100. *Med Phys*. 2007;34(4):1364-1371.
34. Pauwels R, Theodorakou C, Walker A, et al. Dose distribution for dental cone beam CT and its implication for defining a dose index. *Dentomaxillofac Radiol*. 2012;41(7):583-593.
35. Rivera T. Thermoluminescence in medical dosimetry. *Appl Radiat Isot*. 2012;71 Suppl:30-34.
36. Yukihiro EG, McKeever SW. Optically stimulated luminescence (OSL) dosimetry in medicine. *Phys Med Biol*. 2008;53(20):R351-79.
37. Pradhan AS, Lee JI, Kim JL. Recent developments of optically stimulated luminescence materials and techniques for radiation dosimetry and clinical applications. *J Med Phys*. 2008;33(3):85-99.
38. Jursinic PA. Characterization of optically stimulated luminescent dosimeters, OSLDs, for clinical dosimetric measurements. *Med Phys*. 2007;34(12):4594-4604.
39. Stoebe TG, DeWerd LA. Role of hydroxide impurities in the thermoluminescent behavior of lithium fluoride. *J Appl Phys*. 1985;57(6):2217-2220.

40. Jursinic PA. Changes in optically stimulated luminescent dosimeter (OSLD) dosimetric characteristics with accumulated dose. *Med Phys.* 2010;37(1):132-140.
41. Mobit P, Agyingi E, Sandison G. Comparison of the energy-response factor of LiF and Al₂O₃ in radiotherapy beams. *Radiation Protection Dosimetry.* 2006;119(1-4):497-499.
42. Kerns JR, Kry SF, Sahoo N, Followill DS, Ibbott GS. Angular dependence of the nanoDot OSL dosimeter. *Med Phys.* 2011;38(7):3955-3962.
43. Schembri V, Heijmen BJ. Optically stimulated luminescence (OSL) of carbon-doped aluminum oxide (Al₂O₃:C) for film dosimetry in radiotherapy. *Med Phys.* 2007;34(6):2113-2118.
44. Molen A. CBCT machines. http://3dorthodontist.com/CBCT_Machines.html. Accessed 07/22, 2013.
45. Galileos: Operating Instructions Comfort (Sirona Dental Systems Inc., Long Island City, NY, 2012). URL: <http://td.sirona.com/pdf/6118116.pdf>.
46. Ludlow JB, Ivanovic M. Comparative dosimetry of dental CBCT devices and 64-slice CT for oral and maxillofacial radiology. *Oral Surgery, Oral Medicine, Oral Pathology, Oral Radiology and Endodontology.* 2008;106(1):930-938.
47. Pauwels R, Beinsberger J, Collaert B, et al. Effective dose range for dental cone beam computed tomography scanners. *Eur J Radiol.* 2012;81(2):267-271.
48. Rottke D, Patzelt S, Poxleitner P, Schulze D. Effective dose span of ten different cone beam CT devices. *Dentomaxillofac Radiol.* 2013;42(7):20120417.

49. Ferreira CC, Ximenes RE, Garcia CAB, Vieira JW, Maia AF. Total mass attenuation coefficient evaluation of ten materials commonly used to simulate human tissue. *Journal of Physics: Conference Series*. 2010;249(1):012029.
50. Ludlow JB, Davies-Ludlow LE, Brooks SL, Howerton WB. Dosimetry of 3 CBCT devices for oral and maxillofacial radiology: CB mercuray, NewTom 3G and i-CAT. *Dentomaxillofac Radiol*. 2006;35(4):219-226.
51. Johns HE, Cunningham JR. *The physics of radiology*. Charles C. Thomas; 1983.
52. Ma CM, Coffey CW, DeWerd LA, et al. AAPM protocol for 40-300 kV x-ray beam dosimetry in radiotherapy and radiobiology. *Med Phys*. 2001;28(6):868-893.
53. Al Najjar A, Colosi D, Dauer LT, et al. Comparison of adult and child radiation equivalent doses from 2 dental cone-beam computed tomography units. *Am J Orthod Dentofacial Orthop*. 2013;143(6):784-792.
54. Yahnke C. Calibrating the MicroStar (Landauer Inc., Glenwood, Ill, 2009).
55. Roberts JA, Drage NA, Davies J, Thomas DW. Effective dose from cone beam CT examinations in dentistry. *Br J Radiol*. 2009;82(973):35-40.

APPENDICES

Appendix A: Average OSLD Counts - Full Scan, 42mAs, HC/HR

Anatomic Location	OSLD ID	Baseline	#1	#2		#3		
		Avg Reading	Avg Reading	Net Count/3	Avg Reading	Net Count/3	Avg Reading	Net Count/3
Calvarium anterior	34151D	25	4537	1504	9021	1495	13277	1419
Calvarium left	42477T	22	2190	723	4198	669	6495	766
Calvarium posterior	42098X	27	559	178	1074	171	1571	166
Midbrain	44986I	20	2601	860	5076	825	7624	849
Pituitary	46848I	19	8012	2664	15590	2526	23474	2628
Right orbit	29436W	156	8916	2920	17257	2780	25429	2724
Left orbit	48908I	159	10531	3457	20203	3224	29830	3209
Right lens of eye	41606Z	26	3993	1322	7885	1297	13447	1854
Left Lens of eye	46757L	28	9091	3021	18008	2972	26645	2879
Right cheek	409410	25	11283	3753	23137	3951	33587	3483
Right parotid	27592Y	26	20946	6973	41295	6783	61635	6780
Left parotid	37841X	23	22126	7368	43268	7047	64994	7242
Right ramus	26177Z	24	16660	5545	33126	5488	48959	5278
Left ramus	32758P	25	20776	6917	40878	6701	61096	6739
Centre cervical spine	31835W	26	15467	5147	30682	5072	46662	5326
Left back of neck	44131D	26	14888	4954	29766	4959	45804	5346
Right mandible body upper	45032C	27	10287	3420	20686	3466	31160	3491
Right mandible body lower	35299O	158	12480	4107	24701	4074	36750	4016
Left mandible body upper	32817T	27	12404	4126	24570	4055	37065	4165
Left mandible body lower	48629K	160	13443	4428	25831	4129	38810	4326
Right submandibular gland	31657U	162	14824	4887	29631	4936	43213	4527
Left submandibular gland	32871Z	146	16401	5418	31421	5007	47574	5384
Centre sublingual gland	28791V	165	12486	4107	24382	3965	36662	4093
Midline thyroid	46970B	20	2283	754	4495	737	6560	688
Thyroid surface - left	294126	22	1266	415	2639	457	3912	424
Esophagus	35015A	23	2117	698	4084	656	6197	704
Background	321268	21	69	48	70	1	70	0

Appendix B: Average OSLD Counts - Full Scan, HC/HR

<i>Anatomic Location</i>	<i>OSLD ID</i>	Baseline	14 mAs	28 mAs		
		<i>Avg Reading</i>	<i>Avg Reading</i>	<i>Net Count/3</i>	<i>Average Reading</i>	<i>Net Count/3</i>
Calvarium anterior	34151D	57	1305	416	3938	878
Calvarium left	42477T	62	671	203	1878	402
Calvarium posterior	42098X	55	195	47	485	96
Midbrain	44986I	60	818	253	2395	525
Pituitary	46848I	58	2401	781	7383	1661
Right orbit	29436W	55	2687	877	8048	1787
Left orbit	48908I	58	3096	1013	9387	2097
Right lens of eye	41606Z	54	1237	394	3719	827
Left Lens of eye	46757L	62	2816	918	8198	1794
Right cheek	409410	72	3723	1217	11005	2428
Right parotid	27592Y	65	6484	2140	19596	4370
Left parotid	37841X	59	6994	2312	21369	4792
Right ramus	26177Z	61	5221	1720	16129	3636
Left ramus	32758P	63	6212	2050	19539	4442
Centre cervical spine	31835W	59	4862	1601	15085	3408
Left back of neck	44131D	57	4945	1629	15421	3492
Right mandible body upper	45032C	63	3253	1063	9764	2170
Right mandible body lower	35299O	65	3966	1300	12306	2780
Left mandible body upper	32817T	63	3786	1241	11939	2717
Left mandible body lower	48629K	61	4180	1373	12941	2920
Right submandibular gland	31657U	60	4686	1542	14326	3213
Left submandibular gland	32871Z	61	4930	1623	15378	3483
Centre sublingual gland	28791V	56	3957	1300	12006	2683
Midline thyroid	46970B	58	729	223	2288	520
Thyroid surface - left	294126	50	512	154	1322	270
Esophagus	35015A	52	685	211	2100	472
Background	321268	52	56	4	58	2

Appendix C: Average OSLD Counts - Maxillary Scan, HC/HR

Anatomic Location	OSLD ID	Baseline	14 mAs	Net Count/3	28 mAs	Net Count/3	42mAs	Net Count/3
		Avg Reading	Avg Reading		Avg Reading		Avg Reading	
Calvarium anterior	34151D	66	1316	417	4265	983	8417	1384
Calvarium left	42477T	62	691	210	2074	461	4045	657
Calvarium posterior	42098X	61	175	38	462	96	873	137
Midbrain	44986I	63	811	249	2421	537	4845	808
Pituitary	46848I	63	2360	766	7409	1683	14856	2482
Right orbit	29436W	59	2575	839	7924	1783	16181	2752
Left orbit	48908I	60	3115	1018	9538	2141	19056	3173
Right lens of eye	41606Z	65	1379	438	4545	1055	9416	1624
Left Lens of eye	46757L	56	2741	895	8728	1996	17611	2961
Right cheek	40941O	60	3640	1193	11025	2462	22151	3709
Right parotid	27592Y	67	6196	2043	19354	4386	38530	6392
Left parotid	37841X	54	6874	2274	20662	4596	40791	6710
Right ramus	26177Z	59	4965	1635	15084	3373	30711	5209
Left ramus	32758P	69	6055	1995	18960	4302	37425	6155
Centre cervical spine	31835W	62	4630	1523	14174	3181	28433	4753
Left back of neck	44131D	63	1964	633	9152	2396	21077	3975
Right mandible body upper	45032C	59	3109	1017	9533	2141	19199	3222
Right mandible body lower	35299O	60	779	239	2168	463	4122	651
Left mandible body upper	32817T	58	3531	1158	10727	2399	21451	3575
Left mandible body lower	48629K	77	802	242	2541	580	4903	787
Right submandibular gland	31657U	62	1386	441	3935	850	7764	1276
Left submandibular gland	32871Z	63	1465	467	4562	1032	9181	1540
Centre sublingual gland	28791V	61	1035	324	3094	686	6016	974
Midline thyroid	46970B	54	326	91	937	204	1821	295
Thyroid surface - left	294126	60	227	56	591	121	1176	195
Esophagus	35015A	54	342	96	1053	237	2007	318
Background	321268	55	57	1	70	4	57	-4

Appendix D: Average OSLD Counts – Mandibular Scans, HC/HR

<i>Anatomic Location</i>	<i>OSLD ID</i>	Baseline	14 mAs	28 mAs		42mAs		
		<i>Avg Reading</i>	<i>Avg Reading</i>	<i>Net Count/3</i>	<i>Avg Reading</i>	<i>Net Count/3</i>	<i>Avg Reading</i>	<i>Net Count/3</i>
Calvarium anterior	34151D	60	162	34	385	74	732	116
Calvarium left	42477T	67	154	29	370	72	672	101
Calvarium posterior	42098X	57	109	17	210	34	312	34
Midbrain	44986I	64	205	47	559	118	1085	175
Pituitary	46848I	53	371	106	1127	252	2176	350
Right orbit	29436W	65	356	97	872	172	1756	295
Left orbit	48908I	61	372	104	982	203	2022	347
Right lens of eye	41606Z	60	171	37	438	89	866	142
Left Lens of eye	46757L	68	194	42	517	108	973	152
Right cheek	409410	57	3157	1034	7540	1461	14233	2231
Right parotid	27592Y	69	5087	1673	15734	3549	31360	5209
Left parotid	37841X	71	5479	1803	17106	3876	34553	5816
Right ramus	26177Z	72	4417	1448	13677	3087	27206	4510
Left ramus	32758P	70	5552	1828	16783	3743	33672	5630
Centre cervical spine	31835W	74	3650	1192	11708	2686	23121	3805
Left back of neck	44131D	65	4489	1474	14084	3199	27509	4475
Right mandible body upper	45032C	62	2978	972	9192	2071	18736	3181
Right mandible body lower	35299O	59	3885	1276	11812	2642	24356	4181
Left mandible body upper	32817T	70	3512	1147	11156	2548	21446	3430
Left mandible body lower	48629K	65	3744	1226	11981	2746	24373	4131
Right submandibular gland	31657U	66	4279	1404	13393	3038	27137	4581
Left submandibular gland	32871Z	62	4650	1529	14339	3230	29330	4997
Centre sublingual gland	28791V	62	3738	1225	11549	2604	23114	3855
Midline thyroid	46970B	57	638	194	2011	458	4021	670
Thyroid surface - left	294126	58	380	108	1076	232	2117	347
Esophagus	35015A	50	638	196	1760	374	3440	560
Background	321268	48	51	1	62	4	57	-2

Appendix E: Average OSLD Counts – Full Scans

<i>Anatomic Location</i>	<i>OSLD ID</i>	Baseline #1			NC/HR		Baseline #2			HC/NR		NC/NR	
		<i>Avg Reading</i>	<i>Avg Reading</i>	<i>Net Count/3</i>	<i>Avg Reading</i>	<i>Avg Reading</i>	<i>Net Count/3</i>	<i>Avg Reading</i>	<i>Avg Reading</i>	<i>Net Count/3</i>	<i>Avg Reading</i>	<i>Net Count/3</i>	
Calvarium anterior	34151D	3938	7888	1317	60	4793	1577	9179	1462				
Calvarium left	42477T	1878	3873	665	61	2307	748	4459	717				
Calvarium posterior	42098X	485	983	166	70	507	145	1036	177				
Midbrain	44986I	2395	4821	809	63	2642	859	5151	837				
Pituitary	46848I	7383	15020	2546	53	8042	2663	15743	2567				
Right orbit	29436W	8048	16594	2849	61	8602	2847	17043	2814				
Left orbit	48908I	9387	19223	3279	55	10033	3326	19828	3265				
Right lens of eye	41606Z	3719	8339	1540	70	5677	1869	11785	2036				
Left Lens of eye	46757L	8198	17432	3078	60	9376	3105	18130	2918				
Right cheek	409410	11005	21724	3573	60	11908	3949	23086	3726				
Right parotid	27592Y	19596	39577	6660	63	20596	6844	41125	6843				
Left parotid	37841X	21369	45877	8169	61	21888	7276	43055	7056				
Right ramus	26177Z	16129	31607	5159	61	16939	5626	33418	5493				
Left ramus	32758P	19539	39728	6730	66	20044	6659	39572	6509				
Centre cervical spine	31835W	15085	30368	5094	63	15463	5133	30561	5033				
Left back of neck	44131D	15421	31345	5308	61	15083	5007	30760	5226				
Right mand. body upper	45032C	9764	19446	3227	74	10849	3592	21301	3484				
Right mand. body lower	35299O	12306	24222	3972	73	12568	4165	25156	4196				
Left mand. body upper	32817T	11939	23750	3937	64	12267	4068	24397	4043				
Left mand. body lower	48629K	12941	25711	4257	58	13154	4365	26007	4284				
Right submand. gland	31657U	14326	28467	4714	58	14714	4886	29029	4772				
Left submand. gland	32871Z	15378	31108	5243	62	15673	5204	31181	5169				
Centre sublingual gland	28791V	12006	24046	4013	58	12370	4104	24684	4105				
Midline thyroid	46970B	2288	4602	771	56	2173	706	4185	671				
Thyroid surface - left	294126	1322	2677	452	63	1227	388	2542	438				
Esophagus	35015A	2100	4132	677	64	2026	654	3957	644				
Background	321268	58	54	-4	61	60	0	59	0				

CURRICULUM VITAE

Name: David Richard Chambers

Post-secondary Education and Degrees: The University of Western Ontario
London, Ontario, Canada
2011-2014 (expected) M.Cl.D

The University of Western Ontario
London, Ontario, Canada
2000-2004 DDS

The University of Western Ontario
London, Ontario, Canada
1996-2000 H.BSc. Pure Mathematics

Honours and Awards: The Joseph J. and Annie R. Kingston Gold Medal for Pure Mathematics
2000

Continuing Entrance Scholarship, University of Western Ontario
1996-2000

University of Western Ontario Scholarship for Mathematics
1998

Related Work Experience General Dentist, Civilian Contractor
Canadian Forces Bases Borden, Kingston & Trenton
2004-2011